nature geoscience

ARTICLES

https://doi.org/10.1038/s41561-020-00659-z

Check for updates

Coupled anaerobic methane oxidation and reductive arsenic mobilization in wetland soils

Ling-Dong Shi[1], Ting Guo[1], Pan-Long Lv[1], Zi-Fan Niu[1], Yu-Jie Zhou[1], Xian-Jin Tang[1]✉, Ping Zheng[1], Li-Zhong Zhu[1], Yong-Guan Zhu[2], Andreas Kappler[3] and He-Ping Zhao[1]✉

Anaerobic methane oxidation is coupled to the reduction of electron acceptors, such as sulfate, and contributes to their biogeochemical cycling in the environment. However, whether arsenate acts as an alternative electron acceptor of anaerobic methane oxidation and how this influences global arsenic transformations remains elusive. Here, we present incubations of arsenate-contaminated wetland soils from seven provinces in China. Using isotopically labelled methane, we find that anaerobic methane oxidation was linked to arsenate reduction at a rate approaching the theoretical arsenic/methane stoichiometric ratio of 4. In microcosm incubations with natural wetland soils, we find that the coupled pathway of anaerobic methane oxidation and arsenate reduction contributed 26 to 49% of total arsenic release from soils, with arsenic in the more soluble and toxic form arsenite. Comparative gene quantification and metagenomic sequencing suggest that the coupled pathway was facilitated by anaerobic methanotrophs, either independently or synergistically with arsenate-reducing bacteria through reverse methanogenesis and respiratory arsenate reduction. Further bioinformatic analyses show that genes coding for reverse methanogenesis and respiratory arsenate reduction are universally co-distributed in nature. This suggests that coupling of anaerobic methane oxidation and arsenate reduction is a potentially global but previously overlooked process, with implications for arsenic mobilization and environmental contamination.

Arsenic (As) is ubiquitously distributed in aquifers, sediments and soils[1,2], able to cause acute poisoning incidents and chronic cancer-related diseases on humans, wherein As(III) is more noxious than other forms of arsenic in general[3–5]. Arsenic transformation can be mediated by microbial methylation/demethylation[6,7], non-enzymatic co-precipitation[8–10] and abiotic/biotic redox reactions[11]. Microorganisms play a significant role in As conversion and mobilization through reducing As(V) to the more mobile As(III), thus releasing the precipitated As from soils and posing risks to humans and ecosystems[12–15]. Organic matter, including acetate, lactate and humic substances, can stimulate soil-derived As release by promoting microbial arsenate respiration with the enzymatic activity of *arrA* gene[13,16–18].

In addition to these compounds, methane (CH_4) is a naturally widespread organic molecule known to drive microbial reduction of diverse oxidants[19–21]. Anaerobic oxidation of methane (AOM) coupled to sulfate reduction was discovered first in marine sediments[22], syntrophically mediated by anaerobic methanotrophic (ANME) archaea (ANME-1, 2a–c and -3) and sulfate-reducing bacteria[23–25]. Thereafter, members of Methanoperedenaceae have been found to perform AOM coupled to nitrate and metals reduction (Fe(III) and Mn(IV)) without syntrophic partners[26–28]. Other than these known microbial processes, AOM coupled to arsenate reduction (AOM-AsR) is also chemically feasible and thermodynamically favourable (Supplementary Fig. 1)[29], making it conceivable that arsenate may be an overlooked partner of AOM ($\Delta G^0 = -478\,kJ\,mol^{-1}$ CH_4). Although genomic analyses demonstrate the potential of AOM-AsR[30], neither the biological pathway involved in this coupling process nor its possible contribution to geochemical arsenic and carbon cycling is deciphered.

Microbial arsenate reduction exists in natural environments such as paddy soils and wetland sediments, where the potent greenhouse gas methane is highly abundant, with up to approximately 14% of all soil gas and 550 μM of dissolved CH_4 in pore water[1,31,32]. AOM thus has the potential to be coupled to arsenate reduction, enhancing arsenic release. This may further boost As accumulation in plants such as rice not only because of the increased As concentration of exposure, but also due to the better bioavailability of arsenite compared with arsenate[12,33], therefore posing a huge risk to food security[34]. Given the large deposition of arsenic in soils (up to 2.6 billion tonnes per year) and the main species of arsenate[3,35], arsenate reduction coupled to AOM may also represent an important but previously neglected global methane sink.

We therefore hypothesize that AOM can be coupled to arsenate reduction by microorganisms and contributes to arsenic release as well as to the transformation of carbon. We sampled wetland soils to perform both incubations with soil inocula and microcosm incubations, together providing evidence for the naturally widespread occurrence of AOM-AsR and its remarkable but not-yet-reported promotion of soil-arsenic release and global carbon cycling.

AOM-AsR in wetland soils

A total of 19 wetland soils were collected from As-contaminated sites across Southern China (Fig. 1 and Supplementary Dataset 1). The arsenic concentrations in these samples ranged from 9.23 to 7,598.67 $mg\,kg^{-1}$ dry soil, and methane concentrations in pore waters were 2.8–584.1 μM (Supplementary Dataset 2).

Soil samples were inoculated in serum bottles, amended with arsenate and ^{13}C-labelled CH_4, to explore the potential for microbially driven AOM-AsR. During a 7-day incubation, arsenate was significantly reduced to arsenite along with an increase of ^{13}C-labelled dissolved inorganic carbon (^{13}DIC) (Fig. 2a and Extended Data Fig. 1, $P \leq 0.05$). The reduced arsenate was proportional to the

[1]MOE Key Lab of Environmental Remediation and Ecosystem Health, College of Environmental and Resource Sciences, Zhejiang University, Hangzhou, China. [2]Institute of Urban Environment, Chinese Academy of Sciences, Xiamen, China. [3]Center for Applied Geosciences, University of Tübingen, Tübingen, Germany. ✉e-mail: xianjin@zju.edu.cn; zhaohp@zju.edu.cn

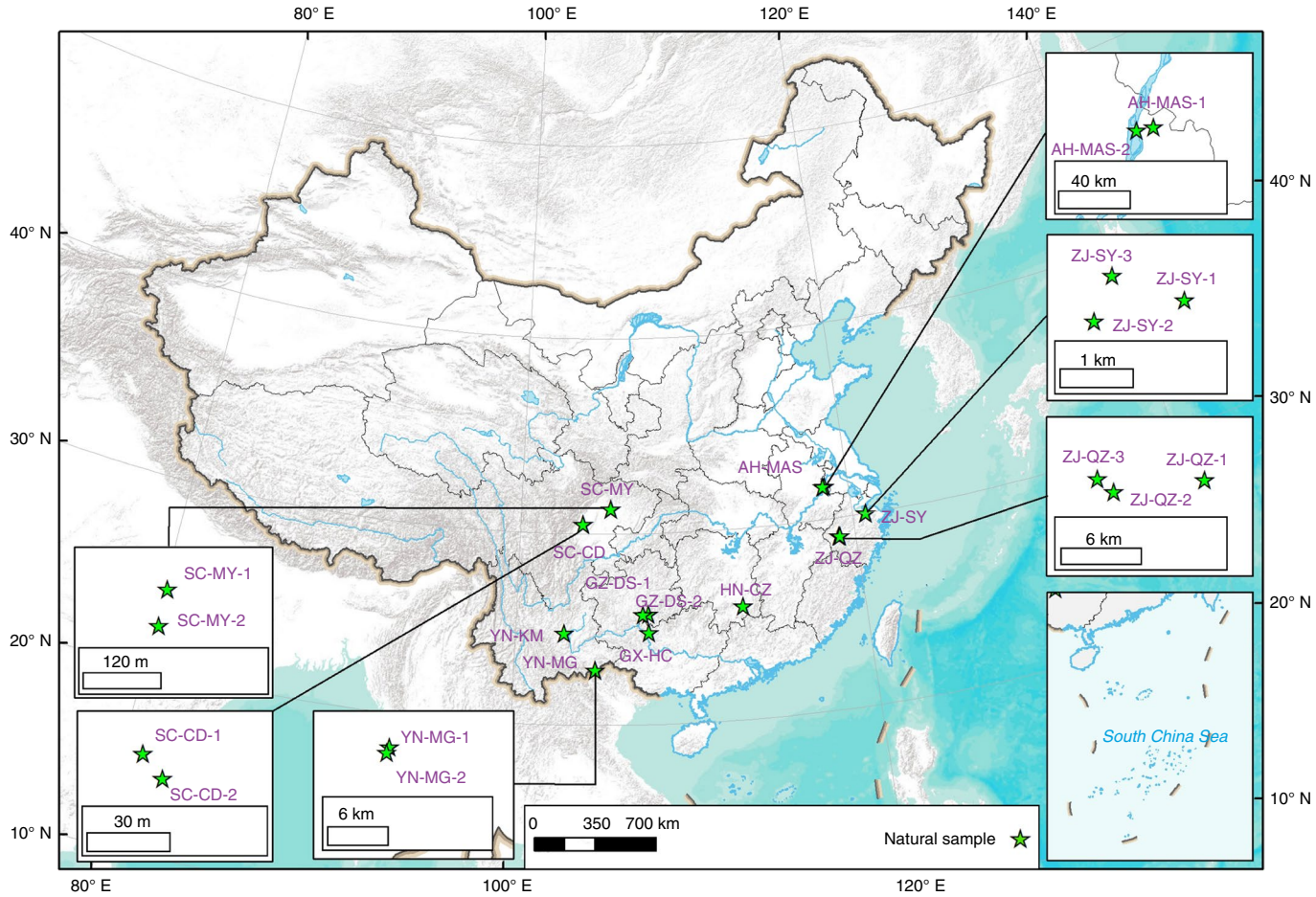

Fig. 1 | Geographic map of field-sampling locations. A total of 19 wetland soils were sampled from 7 provinces in China. Inserts indicate overlapping sampling sites. Detailed geographical locations can be found in Supplementary Dataset 1.

produced ^{13}DIC at an average As/DIC ratio of 3.45 ± 0.50, close to the theoretical ratio of 4 (calculated for oxidation of CH_4 to CO_2 and reduction of As(V) to As(III)), lying within the expected range for AOM-AsR. Other possible electron acceptors, including nitrate, nitrite, sulfate, Fe and Mn, were also measured but were always undetectable or present at trace concentrations. Interestingly, arsenate was also partially reduced in microbially active setups without external addition of CH_4 when inoculated by some samples (Extended Data Fig. 1). One plausible explanation is the presence of redox-active natural organic matter in the soils[36,37], measured as redox potential and dissolved organic carbon (Supplementary Dataset 2). Two samples with a low extent of inherent arsenate reduction in the control setups (non-amended with methane), named AH-MAS-1 and ZJ-SY-1, were selected to further investigate detailed kinetics and stoichiometry of AOM-AsR. When inoculated with AH-MAS-1, the rate of $^{13}CH_4$ oxidation was 2.61 ± 0.20 μM d^{-1}, almost equal to that of ^{13}DIC production at 2.73 ± 0.13 μM d^{-1}, indicating that methane was completely oxidized to carbon dioxide in short-term incubations (Extended Data Fig. 2a). Similarly, the rates of arsenate reduction and arsenite formation were 9.97 ± 0.71 and 9.36 ± 0.34 μM d^{-1}, respectively, showing a nearly complete conversion from arsenate to arsenite (Extended Data Fig. 2b). The ratios of As species to C species were almost identical at ~3.6 (Extended Data Fig. 2c,d), consistent with the average value above. Likewise, the incubation of soil ZJ-SY-1 displayed a very similar trend and relation between methane and arsenate transformation (Supplementary Fig. 2). Combining the results from all soil samples, the rates of arsenate reduction have a significantly positive correlation with that of ^{13}DIC production at a ratio of 3.40 (Fig. 2b, $P < 0.0001$), suggesting that arsenate reduction was strictly dependent on AOM. Taken together, the short-term incubations with methane and arsenate provide direct evidence for the occurrence of AOM-AsR in the wetland soils.

The key functional genes of AOM (ANME-*mcrA*) and arsenate reduction (*arrA*) were quantified in all investigated soils. The absolute abundance of *mcrA* from ANME-1, -2a–c and -2d were in the range of 1.7×10^5–6.0×10^7, 3.5×10^5–4.4×10^8, and 2.1×10^5–9.3×10^7 copies per gram dry soil, respectively, leading to a total of ANME-*mcrA* at 7.3×10^5–5.2×10^8 copies per gram dry soil (Supplementary Fig. 3). The *mcrA* gene of ANME-3 was almost undetectable. The *arrA* gene encoding arsenate reductase ranged from 4.7×10^5 to 6.5×10^7 copies per gram dry soil (Supplementary Fig. 4), comparable to or higher than that of key genes involved in nitrate-, nitrite- and iron-dependent AOM discovered in the ecosystems[31,38,39], as well as ANME-*mcrA*. Moreover, both genes ANME-*mcrA* and *arrA* had a significantly positive correlation with ^{13}DIC production (correlation coefficient $\rho = 0.667$, $P = 0.002$) and arsenate reduction ($\rho = 0.556$, $P = 0.025$), respectively (Extended Data Fig. 3), suggesting that these two genes may be involved in the observed redox processes. Indeed, their transcripts were also detected, with RNA abundance of 2.7×10^5–9.7×10^7 and 5.7×10^4–2.3×10^7 copies per gram dry soil for ANME-*mcrA* and *arrA*, respectively (Supplementary Figs. 3 and 4). The absolute transcription level (ATL) of ANME-*mcrA* was 0.01–2.20, demonstrating its much higher transcriptional activity

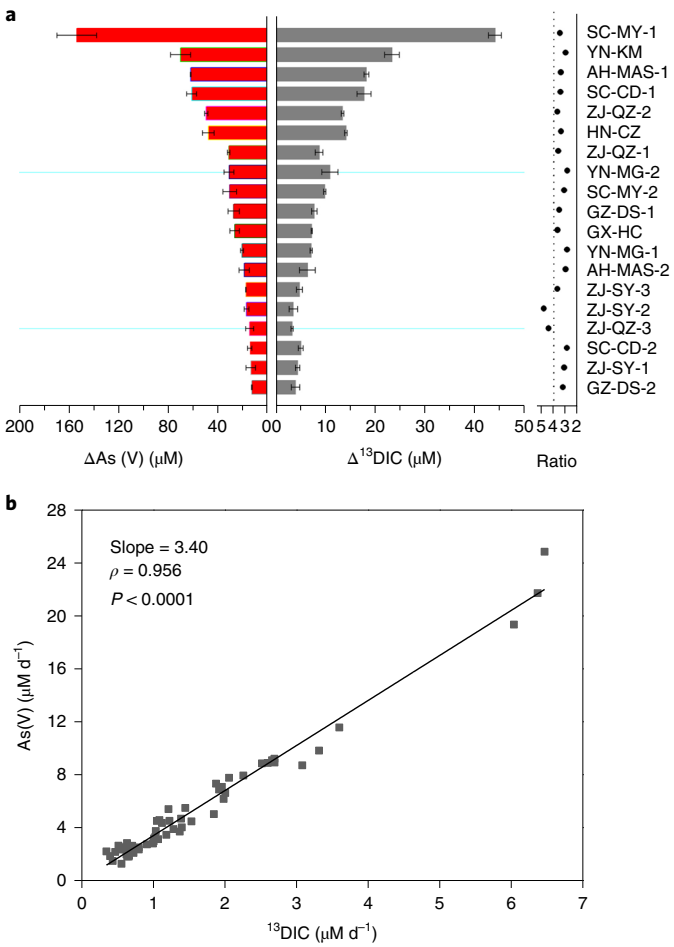

Fig. 2 | Stoichiometry and correlation of As(V) and ^{13}C-DIC concentrations in experiments inoculated by soil samples. a, ΔAs(V) indicates the difference in decreased As(V) concentrations between experiments in the presence or absence of $^{13}CH_4$, while Δ^{13}DIC indicates the difference in increased ^{13}DIC concentrations in the presence or absence of As(V). Error bars indicate standard deviations of triplicate setups. The ratio is calculated as ΔAs(V) divided by Δ^{13}DIC. **b**, ^{13}DIC production and As(V) reduction rates were correlated using Spearman rank correlation. Note that all the replicates are shown separately in the form of individual data points.

than the aerobic methane-oxidation gene *pmoA* of which ATL was only 0.0003–0.13 in the corresponding samples (Supplementary Fig. 5). These transcriptional distinctions, together with the very negative redox potential (Supplementary Dataset 2), indicated that AOM performed by ANME-*mcrA* was the dominantly transcribed pathway for methane oxidation in the investigated ecosystems despite the comparable absolute abundances of *pmoA* gene, implying its possible importance when oxygen was sufficiently available. In addition, *arrA* had a high extent of transcription, with the ATL value of 0.01–1.62 (Supplementary Fig. 4), showing its in situ arsenate-reducing activity.

Physiological pathways of AOM-AsR

To better understand the biological mechanism enabling AOM-AsR, two natural samples containing a high abundance of ANME-*mcrA* and *arrA* (named YN-MG-2 and HN-CZ) were selected for metagenomic sequencing. As expected, *mcrA* genes belonging to ANME-1 and -2 were recovered by metagenomics (Fig. 3). These two groups are well known to couple AOM with the reduction of both soluble oxyanions and poorly soluble iron(III) oxyhydroxides. During AOM-AsR, ANME-1 and ANME-2a–c oxidize methane anaerobically via the reverse methanogenesis pathway catalysed by *mcrA* first[40,41]. The generated electrons are directly transferred to syntrophic sulfate-reducing bacteria, mainly through multi-haem cytochromes (MHCs)[42–45]. In cases of AOM coupled to reduction of Fe(III) and Mn(IV) (oxyhydr)oxide minerals, Methanoperedenaceae members accomplish the redox reactions following a very similar methane activation pathway but without syntrophic partners, reducing the solid electron acceptors by transporting electrons through extracellular MHCs[27,28]. This versatility supports the feasibility of ANME groups participating in AOM-AsR. However, none of *mcrA* affiliated with ANME-3 was detected. This is in line with both the polymerase chain reaction (PCR) results and previous observations that ANME-1 and -2 can inhabit miscellaneous anoxic environments, including marine and freshwater environments, as well as sediments and soils, but ANME-3 was always found in marine methane seeps or submarine mud volcanoes[40].

Microorganisms can reduce solid arsenate (arsenate ions associated with minerals) through the respiratory pathway controlled by the *arrAB* genes encoding a heterodimer consisting of a large catalytic subunit (ArrA) and a small subunit (ArrB)[46]. The subunit ArrA contains a molybdenum-*bis*(pyranopterin guanine dinucleotide) (Mo-*bis*PGD) cofactor and belongs to the dimethyl sulfoxide reductase (DMSOR) superfamily[47]. Phylogenetic analyses of the DMSOR family identified a total of 39 amino acid sequences as potential respiratory arsenate reductases (Fig. 4 and Extended Data Fig. 4). Their downstream coding sequences were extracted, annotated and phylogenetically compared as well; 21 proteins were identified as the small subunit ArrB of respiratory arsenate reductase (Extended Data Fig. 5). By assigning the taxonomy, we finally reconstructed the integrated arsenate reductase (ArrAB) and revealed the most likely affiliations of arsenate reducers (Supplementary Fig. 7). These groups included the well-acknowledged arsenate-reducing genera *Sulfurospirillum* and *Geobacter*[48,49] and other currently unidentified bacterial members.

Overall, metagenomic-based sequencing combined with comparative gene/transcript quantification demonstrated that *mcrA*-based reverse methanogenesis and *arrA*-based anaerobic respiration pathways were transcriptionally active in AOM-AsR. Theoretically, AOM-AsR might be conducted either by individual ANME groups or by syntrophic members. Apparently, bacterial *arrA* genes could be encoded in the genomes of the Methanoperedenaceae family by lateral gene transfer[30], making the former speculation still feasible though arsenate reductase here appeared to be assigned to non-methanotrophs (Extended Data Fig. 6a). The alternative pathway is a syntrophy between methanotrophs and arsenate reducers with MHC as a conceivable accessory link between these two members (Extended Data Fig. 6b) since both groups were reported to perform interspecies electron transfer[50,51]. However, these hypotheses need more evidences from future laboratory studies with enriched or pure microbial cultures.

Arsenic release from coupled AOM-AsR in wetland soils

To explore the ecological influence of AOM-AsR, three representative soils (YN-MG-2, SC-CD-1 and SC-MY-2) with total arsenic contents of 123.7, 69.2 and 9.2 mg kg^{-1} soil were singled out to conduct microcosm incubations (Supplementary Dataset 2). The amendment with $^{13}CH_4$ significantly increased arsenite concentrations in pore waters of all soil samples and concomitantly accumulated $^{13}CO_2$ in the headspace, compared with the control setups with no $^{13}CH_4$ addition (Fig. 5 and Extended Data Figs. 7 and 8, $P \leq 0.05$). Organic arsenic species, including dimethylarsinic acid (DMAs(V)) and monomethylarsonic acid (MMAs(V))[52], were found to be present at trace concentrations, several magnitudes lower than inorganic ones (Supplementary Fig. 8). This was in accordance with the very high conversion of arsenate to arsenite in the experiments

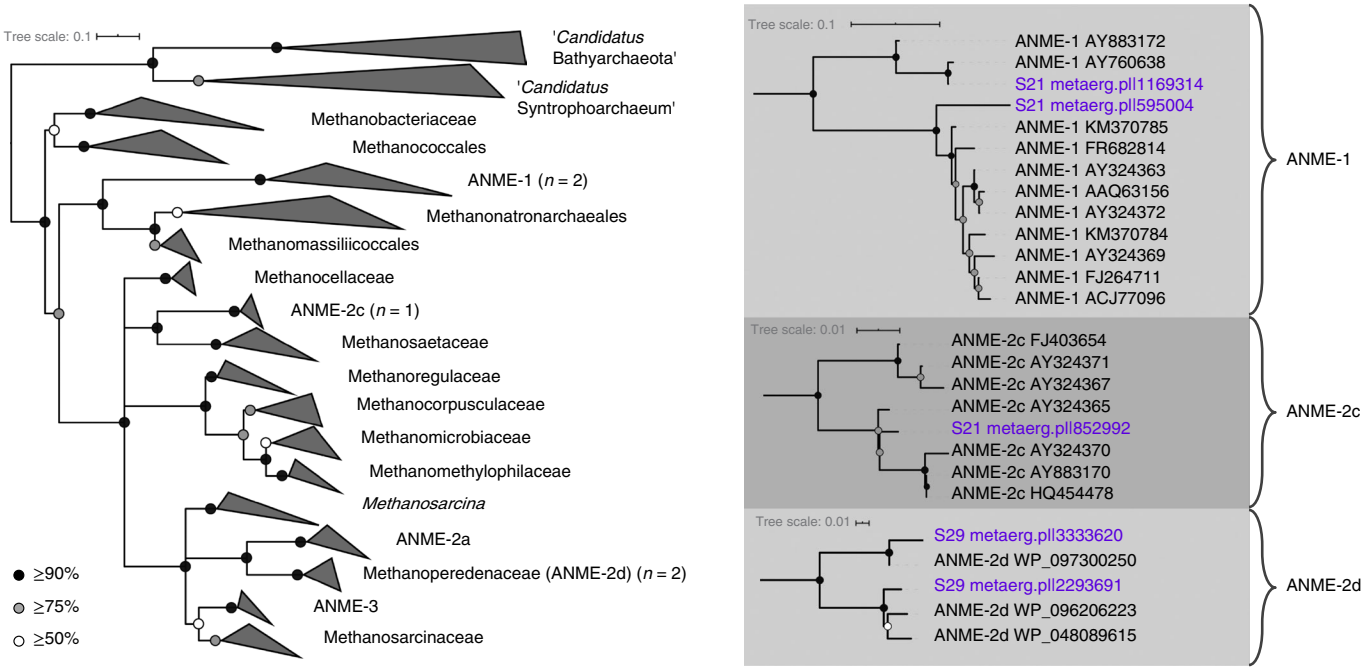

Fig. 3 | Phylogeny of *mcrA* based on amino acid sequences. The numbers of genes related to ANME groups are in bold parentheses. Bootstrap values are generated from 100 replicates; black, grey and white circles show the values ≥90%, ≥75% and ≥50%, respectively. Detailed phylogeny of ANME-*mcrA* recovered in this study (highlighted in purple) and the reference ANME clades are shown on the right side correspondingly. Detailed phylogeny of methanogenic *mcrA*-related sequences is shown in Supplementary Fig. 6. The scale bars represent amino acid changes.

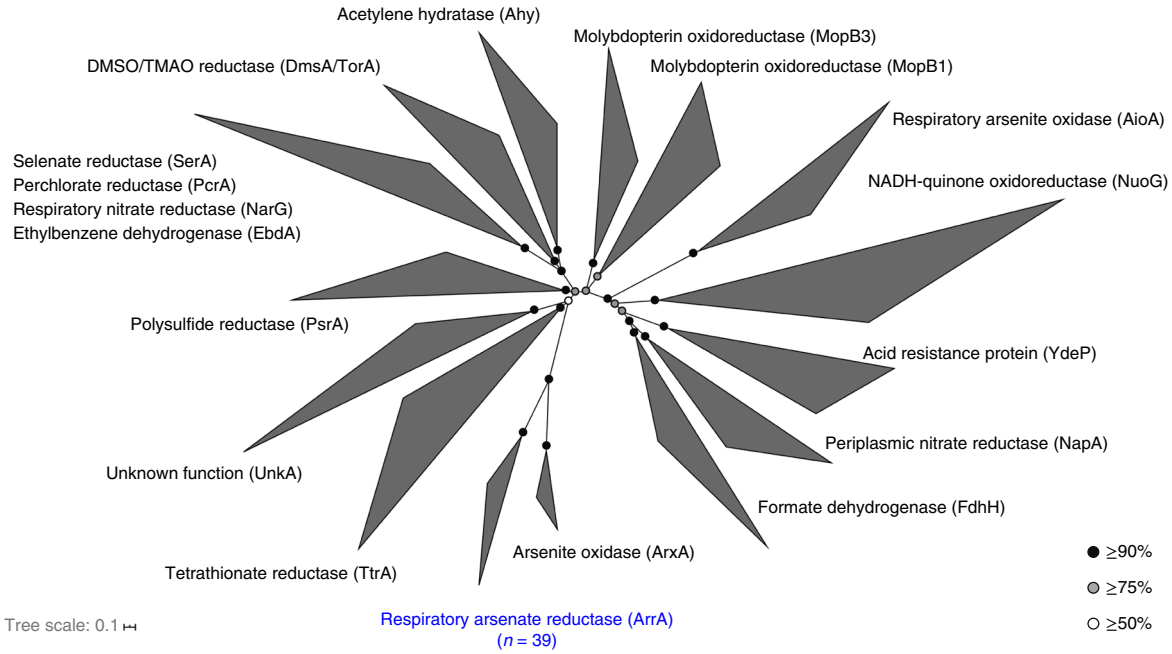

Fig. 4 | Phylogeny of DMSOR superfamily based on amino acid sequences. The numbers of proteins in this study belonging to the respiratory arsenate reductase are shown in parentheses. Bootstrap values are generated from 100 replicates; black, grey and white circles show the values ≥90%, ≥75% and ≥50%, respectively. The scale bar represents amino acid changes. TMAO, trimethylamine N-oxide; NADH, nicotinamide adenine dinucleotide.

inoculated by soil samples and other reports for in situ soil solutions[6]. The partial release of both arsenite and arsenate in the microcosm incubations could be attributed to the microbial transformation using indigenous soil organic carbon and the abiotic dissolution of iron and manganese (oxyhydr)oxides (Extended Data Fig. 8)[36,37,49]. We observed an increase in total Fe, Mn and Fe(II) in the pore water, but without a significant difference between setups amended or unamended with $^{13}CH_4$ (Extended Data Figs. 9 and 10, $P > 0.1$), supporting the abiotic release of arsenite and arsenate. During the incubation of autoclaved soil, neither arsenic nor $^{13}CO_2$ showed a significant difference in the absence or presence of $^{13}CH_4$ (Fig. 5 and Extended Data Figs. 7 and 8, $P > 0.1$). This result,

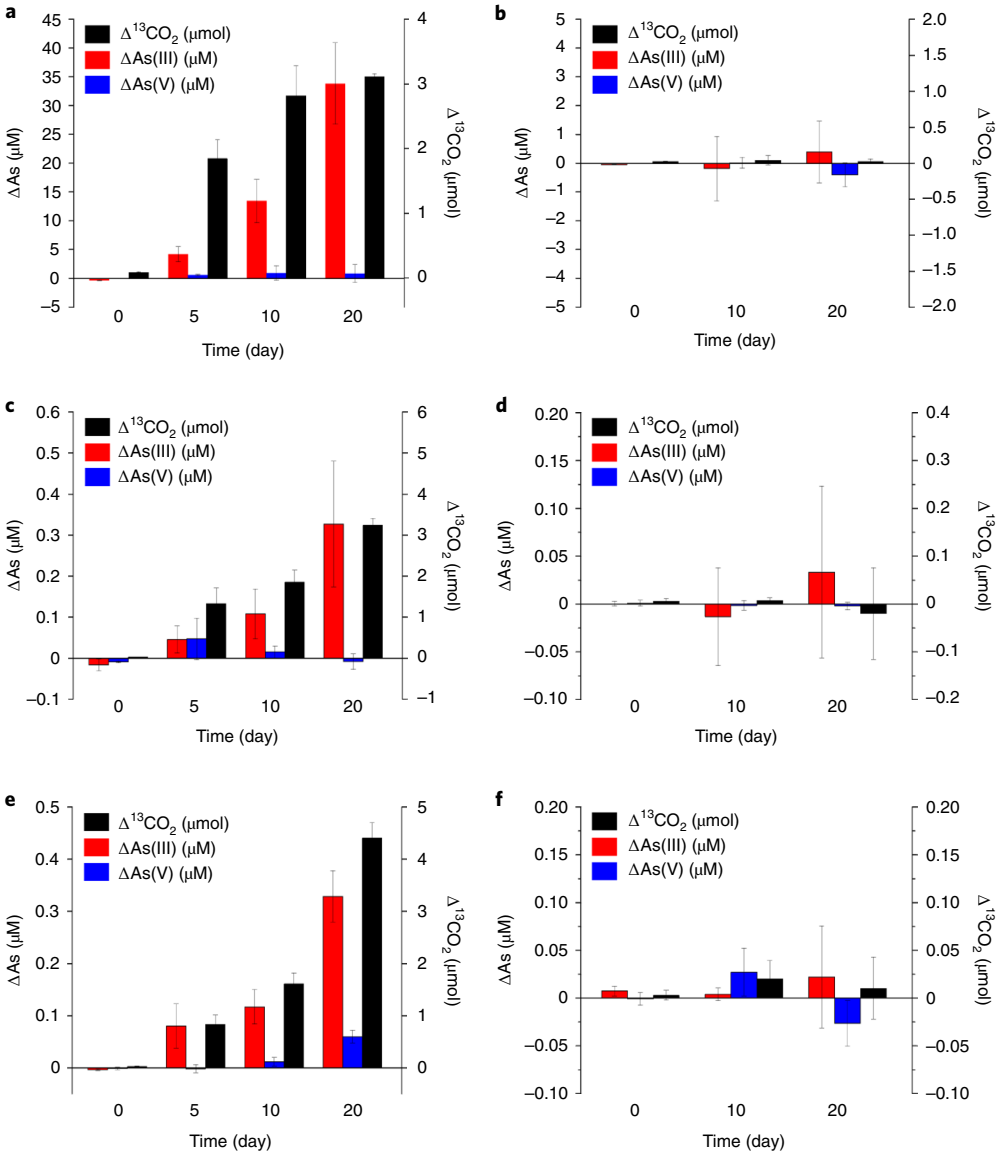

Fig. 5 | Increased dissolved arsenic and gaseous $^{13}CO_2$ of microcosm incubations using representative soils. Arsenic was sampled from the pore water, while $^{13}CO_2$ was in the headspace. Δ values indicate the difference between experimental and control setups (in the presence or absence of $^{13}CH_4$). **a**, YN-MG-2 sample. **c**, SC-CD-1 sample. **e**, SC-MY-2 sample. **b**,**d**,**f**, Corresponding sterile samples (after autoclaving) were used as abiotic controls: YN-MG-2 (**b**), SC-CD-1 (**d**) and SC-MY-2 (**f**). Error bars indicate standard deviations of triplicates. Note that gaseous $^{13}CO_2$ can only be used as an indicator for AOM, and the *y*-axis scales for ΔAs and $\Delta^{13}CO_2$ are different.

together with the production of $^{13}CO_2$ in non-autoclaved incubations, illustrated that the increased portion of dissolved arsenite was probably derived from microbial methane oxidation.

The increased arsenite release could theoretically result from (1) the reduction of arsenate driven by the products of iron- or manganese-dependent AOM (Fe(II) and Mn(II)) or (2) the desorption of arsenic as a consequence of microbial Fe(III) and Mn(IV) mineral dissolution. However, first, both solid-phase associated Fe(II) in the soils (Supplementary Fig. 9) and soluble Fe(II) and Mn(II) (total Mn because only Mn(II) would be dissolved in the soil solution[53]) in the pore waters (Extended Data Figs. 9 and 10) showed no noteworthy difference between the setups with and without $^{13}CH_4$ addition, suggesting that iron and manganese reduction were not methane dependent. Second, total soil Fe and Mn contents and dissolved concentrations in the experimental setups did not significantly differ from those in controls (Extended Data Figs. 9 and 10 and Supplementary Fig. 9, $P > 0.1$), indicating that methane-based microbial dissolution of Fe and Mn precipitates is negligible. Third, mineral leaching would non-selectively release both arsenate and arsenite, whereas the arsenate here was not remarkably different between the two setups (Fig. 5 and Extended Data Fig. 8). In summary, the evidence provided falsified the two possibilities mentioned and further proved that the additional arsenite release was indeed caused by AOM-AsR.

On the basis of microcosm incubations, we estimate that AOM-AsR contributed approximately 33.5%, 26.4% and 49.2% of total arsenic release in YN-MG-2, SC-CD-1 and SC-MY-2 samples (Supplementary Discussion), respectively, suggesting AOM-AsR as a previously overlooked but important pathway for releasing arsenic from wetland soils. However, arsenate reduction would anaerobically consume 6.67‰, 0.073‰ and 0.067‰ of the current methane flux in wetlands, demonstrating AOM-AsR as an important methane sink in arsenic-rich environments probably regulating biogeochemical carbon cycling (Supplementary Discussion).

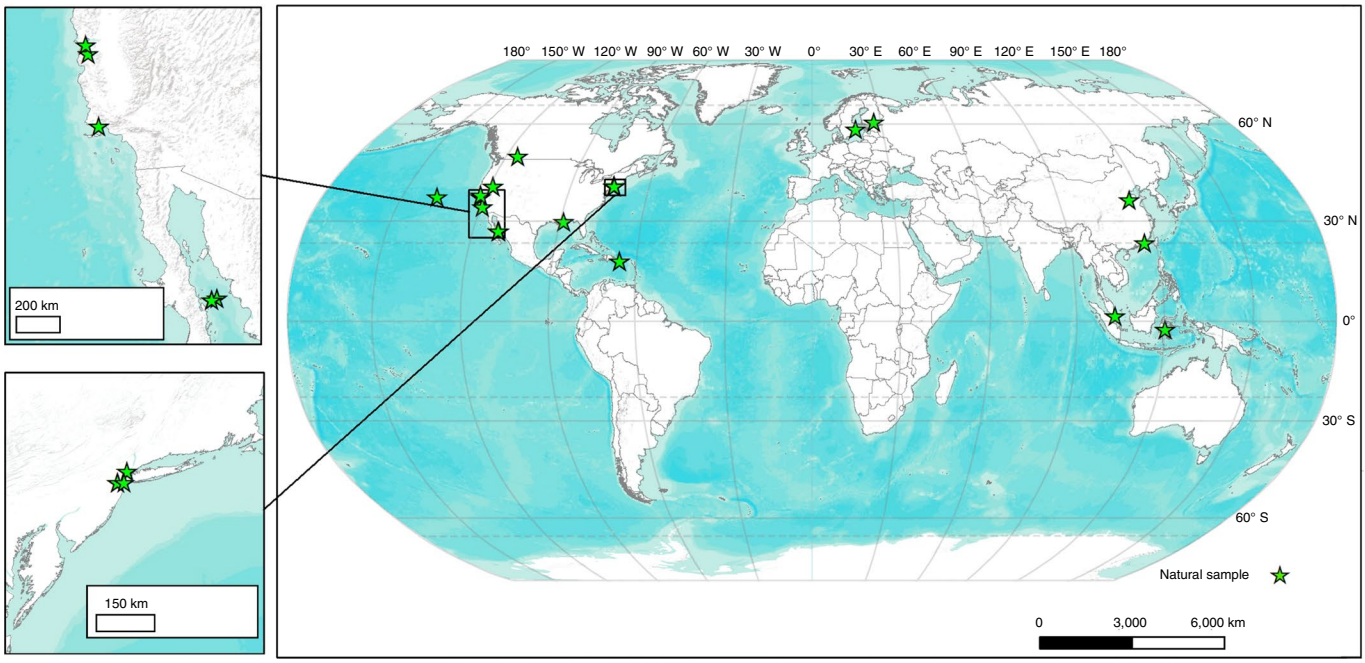

Fig. 6 | Global map with environmental samples containing both ANME-*mcrA* and *arrA* on the basis of bioinformatic prediction. Inserts show detailed location of sampling locations. Geographical information can be found in Supplementary Dataset 3. Note that field samples used in this study are not included.

In addition to trial field samples, we searched and acquired a number of natural samples from public databases, including marine, freshwater and thermal springs sediments, having the potential for AOM-AsR, by using the biomarker of ANME-*mcrA* and *arrA* genes (Fig. 6 and Supplementary Dataset 3). Indeed, some environments (for example, the sediment of Guaymas Basin) were previously found to contain ANME groups enabling sulfate-dependent AOM[54,55], lending more support to the bioinformatic prediction of worldwidely existing AOM-AsR.

AOM coupled to the reduction of sulfate, nitrate/nitrite, iron(III) and manganese(IV) has been well documented. In this study, we provide evidence for a not-yet-reported but widely distributed AOM-AsR . This discovery not only expands our understanding of AOM-coupled processes but also implicates their ecological effect linking to environmental health and biogeochemical cycling of elements.

Online content

Any methods, additional references, Nature Research reporting summaries, source data, extended data, supplementary information, acknowledgements, peer review information; details of author contributions and competing interests; and statements of data and code availability are available at https://doi.org/10.1038/s41561-020-00659-z.

Received: 18 March 2020; Accepted: 15 October 2020;
Published online: 23 November 2020

References

1. Zhu, Y. G., Yoshinaga, M., Zhao, F. J. & Rosen, B. P. Earth abides arsenic biotransformations. *Annu. Rev. Earth Planet. Sci.* **42**, 443–467 (2014).
2. Singh, R., Singh, S., Parihar, P., Singh, V. P. & Prasad, S. M. Arsenic contamination, consequences and remediation techniques: a review. Ecotoxicol. Environ. *Saf.* **112**, 247–270 (2015).
3. Cullen, W. R. & Reimer, K. J. Arsenic speciation in the environment. *Chem. Rev.* **89**, 713–764 (1989).
4. Masscheleyn, P. H., Delaune, R. D. & Patrick, W. H. Effect of redox potential and pH on arsenic speciation and solubility in a contaminated soil. *Environ. Sci. Technol.* **25**, 1414–1419 (1991).
5. Abernathy, C. O., Thomas, D. J. & Calderon, R. L. Health effects and risk assessment of arsenic. *J. Nutr.* **133**, 1536S–1538S (2003).
6. Jia, Y. et al. Microbial arsenic methylation in soil and rice rhizosphere. *Environ. Sci. Technol.* **47**, 3141–3148 (2013).
7. Chen, C. et al. Sulfate-reducing bacteria and methanogens are involved in arsenic methylation and demethylation in paddy soils. *ISME J.* **13**, 2523–2535 (2019).
8. Burton, E. D., Johnston, S. G. & Kocar, B. D. Arsenic mobility during flooding of contaminated soil: the effect of microbial sulfate reduction. *Environ. Sci. Technol.* **48**, 13660–13667 (2014).
9. Bao, P. et al. The role of sulfate-reducing prokaryotes in the coupling of element biogeochemical cycling. *Sci. Total Environ.* **613**, 398–408 (2018).
10. Wolfe, A. L. & Wilkin, R. T. Evidence of sulfate-dependent anaerobic methane oxidation within an area impacted by coalbed methane-related gas migration. *Environ. Sci. Technol.* **51**, 1901–1909 (2017).
11. Amstaetter, K., Borch, T., Larese-Casanova, P. & Kappler, A. Redox transformation of arsenic by Fe(II)-activated goethite (alpha-FeOOH). *Environ. Sci. Technol.* **44**, 102–108 (2010).
12. Ma, J. F. et al. Transporters of arsenite in rice and their role in arsenic accumulation in rice grain. *Proc. Natl Acad. Sci. USA* **105**, 9931–9935 (2008).
13. Zobrist, J., Dowdle, P. R., Davis, J. A. & Oremland, R. S. Mobilization of arsenite by dissimilatory reduction of adsorbed arsenate. *Environ. Sci. Technol.* **34**, 4747–4753 (2000).
14. Macur, R. E., Wheeler, J. T., McDermott, T. R. & Inskeep, W. P. Microbial populations associated with the reduction and enhanced mobilization of arsenic in mine tailings. *Environ. Sci. Technol.* **35**, 3676–3682 (2001).
15. Bruschi, M., Barton, L. L., Goulhen, F. & Plunkett, R. M. in *Sulphate-Reducing Bacteria: Environmental and Engineered Systems* (eds Barton, L. L. & Hamilton, W. A.) 435–458 (Cambridge Univ. Press, 2007).
16. Qiao, J. T. et al. Transcriptional activity of arsenic-reducing bacteria and genes regulated by lactate and biochar during arsenic transformation in flooded paddy soil. *Environ. Sci. Technol.* **52**, 61–70 (2018).
17. Kudo, K. et al. Release of arsenic from soil by a novel dissimilatory arsenate-reducing bacterium, *Anaeromyxobacter* sp. strain PSR-1. *Appl. Environ. Microbiol.* **79**, 4635–4642 (2013).
18. Qiao, J. et al. Humic substances facilitate arsenic reduction and release in flooded paddy soil. *Environ. Sci. Technol.* **53**, 5034–5042 (2019).
19. Milucka, J. et al. Zero-valent sulphur is a key intermediate in marine methane oxidation. *Nature* **491**, 541–546 (2012).
20. Raghoebarsing, A. A. et al. A microbial consortium couples anaerobic methane oxidation to denitrification. *Nature* **440**, 918–921 (2006).
21. Beal, E. J., House, C. H. & Orphan, V. J. Manganese- and iron-dependent marine methane oxidation. *Science* **325**, 184–187 (2009).

22. Devol, A. H. & Ahmed, S. I. Are high rates of sulfate reduction associated with anaerobic oxidation of methane. *Nature* **291**, 407–408 (1981).
23. Niemann, H. et al. Novel microbial communities of the Haakon Mosby mud volcano and their role as a methane sink. *Nature* **443**, 854–858 (2006).
24. Boetius, A. et al. A marine microbial consortium apparently mediating anaerobic oxidation of methane. *Nature* **407**, 623–626 (2000).
25. Orphan, V. J., House, C. H., Hinrichs, K. U., McKeegan, K. D. & DeLong, E. F. Methane-consuming archaea revealed by directly coupled isotopic and phylogenetic analysis. *Science* **293**, 484–487 (2001).
26. Haroon, M. F. et al. Anaerobic oxidation of methane coupled to nitrate reduction in a novel archaeal lineage. *Nature* **500**, 567–570 (2013).
27. Cai, C. et al. A methanotrophic archaeon couples anaerobic oxidation of methane to Fe(III) reduction. *ISME J.* **12**, 1929–1939 (2018).
28. Leu, A. O. et al. Anaerobic methane oxidation coupled to manganese reduction by members of the Methanoperedenaceae. *ISME J.* **14**, 1030–1041 (2020).
29. Caldwell, S. L. et al. Anaerobic oxidation of methane: mechanisms, bioenergetics, and the ecology of associated microorganisms. *Environ. Sci. Technol.* **42**, 6791–6799 (2008).
30. Leu, A. O. et al. Lateral gene transfer drives metabolic flexibility in the anaerobic methane-oxidizing archaeal family *Methanoperedenaceae*. *mBio* **11**, e01325-20 (2020).
31. Ruff, S. E. et al. Methane seep in shallow-water permeable sediment harbors high diversity of anaerobic methanotrophic communities, Elba, Italy. *Front. Microbiol.* **7**, 374 (2016).
32. Hu, B. L. et al. Evidence for nitrite-dependent anaerobic methane oxidation as a previously overlooked microbial methane sink in wetlands. *Proc. Natl Acad. Sci. USA* **111**, 4495–4500 (2014).
33. Muehe, E. M., Wang, T. M., Kerl, C. F., Planer-Friedrich, B. & Fendorf, S. Rice production threatened by coupled stresses of climate and soil arsenic. *Nat. Commun.* **10**, 4985 (2019).
34. Seyfferth, A. L., McCurdy, S., Schaefer, M. V. & Fendorf, S. Arsenic concentrations in paddy soil and rice and health implications for major rice-growing regions of Cambodia. *Environ. Sci. Technol.* **48**, 4699–4706 (2014).
35. Sohn, E. The toxic side of rice. *Nature* **514**, S62–S63 (2014).
36. Das, S., Liu, C. C., Jean, J. S. & Liu, T. L. Dissimilatory arsenate reduction and in situ microbial activities and diversity in arsenic-rich groundwater of Chianan Plain, Southwestern Taiwan. *Microbiol. Ecol.* **71**, 365–374 (2016).
37. Jiang, J., Bauer, I., Paul, A. & Kappler, A. Arsenic redox changes by microbially and chemically formed semiquinone radicals and hydroquinones in a humic substance model quinone. *Environ. Sci. Technol.* **43**, 3639–3645 (2009).
38. Shen, L. D., Ouyang, L., Zhu, Y. & Trimmer, M. Active pathways of anaerobic methane oxidation across contrasting riverbeds. *ISME J.* **13**, 752–766 (2019).
39. Aromokeye, D. A. et al. Rates and microbial players of iron-driven anaerobic oxidation of methane in methanic marine sediments. *Front. Microbiol.* **10**, 3041 (2020).
40. Wang, F. P. et al. Methanotrophic archaea possessing diverging methane-oxidizing and electron-transporting pathways. *ISME J.* **8**, 1069–1078 (2014).
41. Hallam, S. J. et al. Reverse methanogenesis: testing the hypothesis with environmental genomics. *Science* **305**, 1457–1462 (2004).
42. Wegener, G., Krukenberg, V., Riedel, D., Tegetmeyer, H. E. & Boetius, A. Intercellular wiring enables electron transfer between methanotrophic archaea and bacteria. *Nature* **526**, 587–590 (2015).
43. McGlynn, S. E., Chadwick, G. L., Kempes, C. P. & Orphan, V. J. Single cell activity reveals direct electron transfer in methanotrophic consortia. *Nature* **526**, 531–535 (2015).
44. Scheller, S., Yu, H., Chadwick, G. L., McGlynn, S. E. & Orphan, V. J. Artificial electron acceptors decouple archaeal methane oxidation from sulfate reduction. *Science* **351**, 703–707 (2016).
45. Kletzin, A. et al. Cytochromes *c* in Archaea: distribution, maturation, cell architecture, and the special case of *Ignicoccus hospitalis*. *Front. Microbiol.* **6**, 439 (2015).
46. Zhu, Y. G., Xue, X. M., Kappler, A., Rosen, B. P. & Meharg, A. A. Linking genes to microbial biogeochemical cycling: lessons from arsenic. *Environ. Sci. Technol.* **51**, 7326–7339 (2017).
47. Shi, L. D. et al. Multi-omics reveal various potential antimonate reductases from phylogenetically diverse microorganisms. *Appl. Microbiol. Biotechnol.* **103**, 9119–9129 (2019).
48. Ahmann, D., Roberts, A. L., Krumholz, L. R. & Morel, F. M. M. Microbe grows by reducing arsenic. *Nature* **371**, 750 (1994).
49. Tian, H. X., Shi, Q. T. & Jing, C. Y. Arsenic biotransformation in solid waste residue: comparison of contributions from bacteria with arsenate and iron reducing pathways. *Environ. Sci. Technol.* **49**, 2140–2146 (2015).
50. Shi, L. et al. Extracellular electron transfer mechanisms between microorganisms and minerals. *Nat. Rev. Microbiol.* **14**, 651–662 (2016).
51. Lovley, D. R. & Malvankar, N. S. Seeing is believing: novel imaging techniques help clarify microbial nanowire structure and function. *Environ. Microbiol.* **17**, 2209–2215 (2015).
52. Zhao, F. J., Ma, J. F., Meharg, A. A. & McGrath, S. P. Arsenic uptake and metabolism in plants. *New Phytol.* **181**, 777–794 (2009).
53. Bao, S. D. *Soil Agrochemical Analysis* 3rd edn (China Agricultural Press, 2011).
54. Teske, A. et al. Microbial diversity of hydrothermal sediments in the Guaymas Basin: evidence for anaerobic methanotrophic communities. *Appl. Environ. Microbiol.* **68**, 1994–2007 (2002).
55. Biddle, J. F. et al. Anaerobic oxidation of methane at different temperature regimes in Guaymas Basin hydrothermal sediments. *ISME J.* **6**, 1018–1031 (2012).

Methods

Sample collections. A total of 19 natural wetland samples distributed in 7 provinces in southern China were collected from the upper 20 cm during June and July 2019, as shown in Supplementary Dataset 1 and Fig. 1, which was drawn by ArcGIS 10.2. The names denote the province, city and site of the sample sources. For example, ZJ-SY-1 means that this sample was taken from one site in Shangyu, Zhejiang Province. The detailed location is in the Supplementary Dataset 1. For each site, five soil samples were collected into gas-tight bags and then mixed to make a composite sample. Approximately 1–2 kg composite soil samples were placed into bigger sealed plastic bags and immediately transferred to the lab on ice for downstream analysis.

Measurement of soil properties. For total Fe, Mn and As, the field samples were digested with an acid mixture of HNO_3, HF and H_2O_2 (volume ratio = 4/2/2). The concentrations of total Fe, Mn and As were determined using inductively coupled plasma mass spectrometer (ICP-MS) (NEXION300XX, PerkinElmer). Elementary points of analytical process including certified reference materials, and interferences were fully considered to guarantee the quality of the analyses. The solution after microwave digestion was heated at 140 °C to almost dryness using a heater (SZ-BHW-09C20, Botong Chemical Technology) to remove the excess acid and therefore to reduce the effect of HF on ICP-MS analysis. To reduce the physical interference, the residual solution was diluted and filtered through a 0.45 μm filter to remove the total dissolved solids in the solution. When measuring the total As by ICP-MS, kinetic energy discrimination (KED) mode colliding with He gas was used to remove the interference of polyatomic ions. The argon nebulizer gas flow was 0.89 l min^{-1}. To ensure the best performance of the ICP-MS and to reduce the interferences of oxide ions and doubly charged ions, daily performance checks and optimization, including torch alignment, nebulizer gas flow standard (STD)/KED (NEB) and autolens STD/dynamic reaction cell (DRC) mode were conducted. Eight multi-element samples (containing As, Fe and Mn) were used as calibration standards. The correlation coefficient value for the standard curve was found to be above 0.999. When measuring, 40 μg l^{-1} internal standard rhodium (Rh) was added for quality control, and Rh recovery was 80–120%. Standard soil reference (GBW07443(GSF-3)) prepared by the Geophysiochemistry Prospecting Institute of the Academy of Geological Science of China was also digested and measured. The recoveries of standard reference materials were within the range of 97–102%, which demonstrated that the method for detection was credible.

The total nitrogen (TN), total carbon (TC) and total sulfur contents in the samples were measured using an element analyser (Elementar Vario EL Cube). For the total organic carbon determination, a 70 mg sample was weighed in a ceramic boat and acidified with 1 M HCl to remove inorganic carbon. The samples were then dried and measured with a TN/TC analyser (Analytik Jena multi N/C 3100). Dissolved organic carbon and dissolved organic nitrogen of soils and sediments were extracted with Milli-Q water at a ratio of 1/5 (w/v) and then measured with the same TN/TC analyser. Moisture content (m%) was determined by putting approximately 20 g (m_1) of wet soil samples in an oven drying at 105 °C for 12 hours until the weight kept constant (m_2), according to the following equation:

$$m\% = (m1 - m2)/m2 \times 100\%.$$

For the determination of soil mechanical composition, 50.0 g of 2 mm sieved soil was weighted and shaken inside a 500 ml triangular flask with 250 ml of distilled water and dispersant. After stewing for 2 hours, the suspension was heated and boiled for 1 hour. Finally, it was transferred to a 1 l sedimentation cylinder to determine the grain size by wet sieving and the hydrometer apparatus. By reading the hydrometer and temperature, sand (0.020–2.000 mm), silt (0.002–0.020 mm) and clay (<0.002 mm) percentage content was determined. The pH and oxidation–reduction potential (ORP) of soils were directly measured in situ by pH meter and ORP meter.

For the measurement of methane in pore waters, approximately 20.0 g of wetland soil was added to 120 ml serum bottles containing 50 ml of saturated NaCl solution. Bottles were sealed immediately with butyl-rubber stoppers and a crimp seal. After thorough mixing, methane in the headspace was measured using gas chromatogram (GC 7890A, Agilent). The dissolved methane in the liquid was calculated by Henry's law on the basis of the gaseous concentration. The total methane in the pore water was the sum of that in the headspace and liquid and was further divided by the pore-water volume to generate the methane concentration in pore waters.

Incubations with soil inocula. The mineral medium contained NH_4Cl 0.02 g, $CaCl_2$ 1 mg, $NaHCO_3$ 0.3 g, $MgCl_2$ 2 mg, $MgSO_4{\cdot}7H_2O$ 0.2 mg, KH_2PO_4 0.2 g, $Na_2HPO_4{\cdot}12H_2O$ 0.4 g, 1 ml acid trace element solution (HCl 100 mmol, $FeCl_2{\cdot}4H_2O$ 1.49 g, $ZnCl_2$ 32.2 mg, H_3BO_3 14 mg, $CoCl_2{\cdot}6H_2O$ 120 mg, $MnCl_2{\cdot}4H_2O$ 500 mg, $CuCl_2$ 270 mg, $NiCl_2{\cdot}6H_2O$ 95 mg per litre) and 1 ml alkaline trace element solution (NaOH 10 mmol, SeO_2 67 mg, $Na_2WO_4{\cdot}2H_2O$ 50 mg, $Na_2MoO_4{\cdot}2H_2O$ 242 mg per litre) in 1 l of demineralized water. After complete dissolution, the medium was autoclaved for 20 minutes. Approximately 0.50 g of collected dry soils and 50 ml of mineral medium were incubated into 60 ml serum bottles and degassed using argon for 20 minutes (Supplementary Fig. 10). The stock solution of arsenate (15 mM of $Na_2HAsO_4{\cdot}7H_2O$, Sigma-Aldrich), after degassing with argon, was added to make the initial As concentration at approximately 70 μM and replenished once consumed completely. Serum bottles were then tightly closed with butyl-rubber stoppers and sealed with crimped aluminium caps. Finally, 0.2 ml of ^{13}C-labelled CH_4 was injected to maintain methane content at an environmentally relevant concentration of ~2% (v/v) in the headspace[32]. The remaining dissolved oxygen was determined below the limit of detection of 1 μM, calculated by Henry's law according to the measured oxygen in headspace, using gas chromatography (Agilent 7890 A) configured with an HP-PLOT Molesieve column. The bottles were incubated upside down in a dark shaker at 25 °C and 150 rpm for 7 days. The residual oxygen (1 μM) combined with the possibly maximum diffused oxygen through rubber stoppers (91 nM in 7-day operation) would account for at most only 16.7% of oxidized CH_4 (3.3 μM in the ZJ-QZ-3 sample, Fig. 2a) and for a range of 1.2–16.7% in all the samples, given 2 mol O_2 required for oxidizing 1 mol CH_4[56]. Every soil sample had two control experimental setups: one set-up was prepared in the absence of arsenate and the other one in the absence of $^{13}CH_4$. All other conditions were identical to those in the experimental setups. Each set-up has three replicates.

On days 0, 1, 3, 5 and 7, liquid samples were taken over time and filtrated by 0.22 μm filter membranes immediately for the downstream measurements. Arsenate was measured using ion chromatography equipped with a conductivity detector and AS19 separation column (Dionex ICS-1000, Thermo Scientific), while arsenite was first oxidized by 30% H_2O_2. The eluent concentration and flow rate were set at 20 mM KOH and 1 ml min^{-1}, respectively. The limit of detection for arsenate was 1 μM, and the precision was at a relative standard deviation <1.0%. The $^{13}CH_4$ and $^{13}CO_2$ in the headspace were quantified accordingly using gas chromatography–mass spectrometry (GC 7890 A coupled to MSD 5977B, Agilent). Total $^{13}CO_2$ in the liquid ($^{13}CO_2 + {}^{13}HCO_3^- + {}^{13}CO_3^{2-}$) was measured using isotope-ratio mass spectrometry (MAT 253, Thermo Scientific). Briefly, water samples were first injected into evacuated septa tubes with phosphoric acid. The released CO_2 gas was then analysed to report the stable isotopic results. We used the term ^{13}DIC to designate the total quantity of produced $^{13}CO_2$ both in the headspace and in the liquid and normalized by total medium volume. In addition, dissolved nitrate, nitrite and sulfate were measured using the identical ion chromatography at KOH eluent concentration of 15 mM. Total iron and manganese ions were measured using ICP-MS as described previously. The limits of detection of nitrate, nitrite, sulfate, iron and manganese are 0.5, 0.8, 1.0, 0.03 and 0.03 μM, respectively.

Nucleic acid extraction and quantification. Microbial DNA was extracted from the field samples (0.5 g) using the FastDNA SPIN Kit for Soil (MP Biomedicals). Total RNA was extracted by RNeasy PowerSoil Kit (QIAGEN) following the manual. Purity and concentration of DNA and RNA were assessed with a NanoDrop spectrophotometer (ND-1000).

Reverse transcription and quantitive polymerase chain reaction. Up to now, there are no universal primers to amplify the genes of anaerobic methane oxidation (*mcrA*) for all the anaerobic methanotrophs (ANME-1 to -3). Thus, primers Type a-b (forward: 5′-TGGTTCGGAACGTACATGTC-3′; reverse: 5′-TCTYYT CCAGRATGTCCATG-3′), Type c-d (forward: 5′-GCTCTACGACCAGATMTGG CTTGG-3′; reverse: 5′-CCGTAGTACGTGAAGTCATCCAGCA-3′), McrA 159F-345R (Forward: 5′-AAAGTGCGGAGCAGCAATCACC-3′; Reverse: 5′-TCGTCCCATTCCTGCTGCATTGC-3′) and Type e (Forward: 5′-CHCTG GAAGATCACTTCGGTGGTTC-3′; Reverse: 5′-RTATCCGAAGAARCCSAGT CKRCC-3′) were used to target *mcrA* in ANME-1, ANME-2a–c, ANME-2d and ANME-3, respectively[57,58]. Primers AS1 (forward: 5′-CGAAGTTCGTCCCG ATHACNTGG-3′; reverse: 5′-GGGGTGCGGTCYTTNARYTC-3′) were used to amplify the gene for respiratory arsenate reduction (*arrA*)[59]. Primers A189F-MB661R (forward: 5′-GGNGACTGGGACTTCTGG-3′; reverse: 5′-CCGGMGCAACGTCYTTACC-3′) were used to amplify the gene for aerobic methane oxidation (*pmoA*)[60]. Plasmids containing the target gene fragments were used to produce calibration curves. Three replicate polymerase chain reactions using extracted DNA as the template were performed for all samples as previously described[61]. The amplification efficiencies were between 88.9% and 98.5%.

To quantify the transcript abundance, reverse transcription was first performed. The reaction mixture contained reverse transcriptase, dNTP mixture, RNase inhibitor, random primer 6-mers, reaction buffer and the extracted RNA samples. The protocols were 42 °C for 60 min, 70 °C for 15 min and 4 °C until the subsequent use. After obtaining the cDNA, we performed similar quantitative polymerase chain reactions as described in the preceding. The ATL of functional genes was further calculated to indicate their transcriptional activity[62] using the following equation:

$$\mathrm{ATL} = \frac{\text{Transcript abundance (copies per gram dry soil)}}{\text{Gene abundance (copies per gram dry soil)}}$$

Metagenomic sequencing and analysis. Extracted DNA was used for metagenomic sequencing using Illumina HiSeq X Ten (2 × 150 bp), finally

generating ~181 million and ~192 million paired-end reads for YN-MG-2 and HN-CZ, respectively. The low-quality reads were first trimmed or removed by Trimmomatic (v.0.36) using the default parameters[63]. Briefly, the Trimmomatic cut the reads if the average quality within the sliding window fell below the setting threshold. The window size and the quality threshold were set as 4 bases and 15, respectively. In addition, the trimmed reads shorter than 36 bp were discarded. Qualified reads were then assembled individually using MEGAHIT (v.1.1.1)[64]. After removing the contigs of a length of <500 bp, we finally obtained totals of 2,330,913 and 2,635,219 contigs for two samples, of which N50 were 1,049 bp and 861 bp, respectively. Assembled genes were predicted and annotated preliminarily using MetaErg (v.1.2.0)[65].

To identify respiratory arsenate reductase more sufficiently, HMMER (v.3.2.1) with a cut-off e value $\leq 1 \times 10^{-50}$ was performed to search potential proteins against the assembled contigs through a hidden Markov model (HMM) constructed using known reference sequences (Supplementary Table 1)[66,67]. Identified proteins were aligned with reference DMSOR superfamily reductases using MUSCLE (v.3.8.1551), followed by the construction of a phylogenetic tree using FastTree (v.2.1.11) with the WAG + GAMMA models[68,69], to further validate their annotations. Similarly, the downstream sequences of identified putative arsenate reductase genes were also aligned and phylogenetically compared with references using the same tool. The protein encoding sequences, not clustered to the group of respiratory arsenate reductase beta subunit, were removed. Finally, a total of 21 operons containing both alpha and beta subunits of respiratory arsenate reductase were recovered. The taxonomy of genes was considered to be identical to that of the corresponding contig. The contig was assigned to the taxon if more than 50% of its open reading frames belonged to the same phylum/class/order/family/genus[70] using the MetaErg databases[65].

To identify genes encoding methyl-coenzyme M reductase, hmmsearch was performed with a cut-off e value of 10^{-5} and the HMM (PF02249 for *mcrA*) downloaded from the Pfam database[71]. Identified putative McrA sequences were aligned and built for the phylogenetic tree along with other references (Fig. 3), as described in the preceding.

Microcosm incubations. The soil samples were placed in a shady and ventilated indoor place without exposure to the sun, acid, alkali, other gases and dust pollution. The samples were air dried for 5–7 days[53]. Approximately 25.0 g of three dry wetland soils (YN-MG-2, SC-CD-1 and SC-MY-2) through 10-mesh sieve were incubated into 120 ml serum bottles and then flooded with 50 ml anoxic Milli-Q water (Supplementary Fig. 11). The headspace was further degassed using N_2 for 10 min to remove oxygen and immediately sealed with Teflon-coated butyl-rubber stoppers and aluminium crimp seals. Two comparative groups with the addition of 5 ml $^{13}CH_4$ or Ar (10%, v/v) were set up. After measuring the concentrations of $^{13}CH_4$ and $^{13}CO_2$ in the headspace (see the preceding method), triplicate soils of each set-up were destructively sampled, after incubation for 0, 5, 10 and 20 days, to measure the following characteristics of soil and water samples. We extracted DNA and RNA from soil samples, quantified gene abundances and transcript abundances of ANME-*mcrA*, *pmoA*, and *arrA*, following the protocols described above. The ORP of soils was directly measured in situ by an ORP meter at <−200 mV, indicating anoxic conditions. Pore waters acidified with 6 M HCl to prevent As transformation were sampled by centrifuging soils for 10 min at 3,100 × *g*. Concentrations of total Fe and Mn in pore waters were determined with ICP-MS (see the preceding). Fe(II) was measured spectrophotometrically using phenanthroline[72]. Arsenic species were determined by high-performance liquid chromatography (HPLC) ICP-MS (NEXION300XX, PerkinElmer) using an anion exchange PRP X-100 HPLC column (250 × 4.1 mm I.D., 10 µm, Hamilton) and a chromatographic mobile phase of 20 mM $(NH_4)H_2PO_4$ (pH 6.5). Before As species analysis, the ICP-MS was checked and optimized as described in the preceding. Dynamic reaction cell mode was adapted to remove the polyatomic interference here. Five mixed standard samples (1 µg l^{-1}, 10 µg l^{-1}, 20 µg l^{-1}, 50 µg l^{-1} and 100 µg l^{-1}) containing As(III), As(V), DMAs(V) and MMAs(V) were used for the standard curve, with the coefficient value of each As species above 0.999. The pore-water samples were diluted to the allowed scope of As species determination, which was also filtered through a 0.22 µm filter to prevent the blocking of the exchange column in the HPLC. One standard sample of 50 µg l^{-1} was determined every ten samples to control the quality. The recovery of the standard sample was 96–104%, which was considered to be acceptable. The same characteristics of soils were measured as well after digesting first.

In addition, three corresponding soil samples were autoclaved and incubated with $^{13}CH_4$ or argon as described in the preceding to test the abiotic contribution. All the microcosm incubations were performed in triplicate at 25 °C in a dark chamber (without shaking), simulating the in situ conditions of southern China, which showed average temperatures ranging from 10 to 26 °C throughout the year[73].

Bioinformatic predictions. Reference amino acid sequences of methanotrophic McrA and ArrA were used to search target proteins against the non-redundant protein database of MGnify (2019.05), formerly known as EBI Metagenomics, using Diamond (v.0.9.18) with more-sensitive mode and other default parameters (for example, maximum e value of 10^{-5}, minimum query coverage of 50%)[74,75]. Target proteins were filtered with minimum identity of 80% and then linked to assemblies and finally to samples. Only samples having latitude and longitude information were extracted and plotted on the global map using ArcGIS 10.2.

Data availability

All the metagenomic sequencing data have been submitted to the Sequence Read Archive, with BioProject accession number of PRJNA612595. The source data have been deposited into the Open Science Framework (OSF) at https://doi.org/10.17605/OSF.IO/N4SEF. Source data are provided with this paper.

References

56. Oswald, K. et al. Aerobic gammaproteobacterial methanotrophs mitigate methane emissions from oxic and anoxic lake waters. *Limnol. Oceanogr.* **61**, S101–S118 (2016).
57. Nunoura, T. et al. Quantification of *mcrA* by quantitative fluorescent PCR in sediments from methane seep of the Nankai Trough. *FEMS Microbiol. Ecol.* **57**, 149–157 (2006).
58. Vaksmaa, A., Jetten, M. S. M., Ettwig, K. F. & Lüke, C. McrA primers for the detection and quantification of the anaerobic archaeal methanotroph '*Candidatus* Methanoperedens nitroreducens'. *Appl. Microbiol. Biotechnol.* **101**, 1631–1641 (2017).
59. Song, B., Chyun, E., Jaffe, P. R. & Ward, B. B. Molecular methods to detect and monitor dissimilatory arsenate-respiring bacteria (DARB) in sediments. *FEMS Microbiol. Ecol.* **68**, 108–117 (2009).
60. Paszczynski, A. J. et al. Proteomic and targeted qPCR analyses of subsurface microbial communities for presence of methane monooxygenase. *Biodegradation* **22**, 1045–1059 (2011).
61. Zhao, H. P. et al. Interactions between perchlorate and nitrate reductions in the biofilm of a hydrogen-based membrane biofilm reactor. *Environ. Sci. Technol.* **45**, 10155–10162 (2011).
62. Freitag, T. E. & Prosser, J. I. Correlation of methane production and functional gene transcriptional activity in a peat soil. *Appl. Environ. Microbiol.* **75**, 6679–6687 (2009).
63. Bolger, A. M., Lohse, M. & Usadel, B. Trimmomatic: a flexible trimmer for Illumina sequence data. *Bioinformatics* **30**, 2114–2120 (2014).
64. Li, D. et al. MEGAHIT v1.0: a fast and scalable metagenome assembler driven by advanced methodologies and community practices. *Methods* **102**, 3–11 (2016).
65. Dong, X. L. & Strous, M. An integrated pipeline for annotation and visualization of metagenomic contigs. *Front. Genet.* **10**, 999 (2019).
66. Eddy, S. R. Accelerated profile HMM searches. *PLoS Comput. Biol.* **7**, e1002195 (2011).
67. Saunders, J. K., Fuchsman, C. A., McKay, C. & Rocap, G. Complete arsenic-based respiratory cycle in the marine microbial communities of pelagic oxygen-deficient zones. *Proc. Natl Acad. Sci. USA* **116**, 9925–9930 (2019).
68. Price, M. N., Dehal, P. S. & Arkin, A. P. FastTree 2—approximately maximum-likelihood trees for large alignments. *PLoS ONE* **5**, e9490 (2010).
69. Edgar, R. C. MUSCLE: multiple sequence alignment with high accuracy and high throughput. *Nucleic Acids Res.* **32**, 1792–1797 (2004).
70. Ma, L. P. et al. Metagenomic assembly reveals hosts of antibiotic resistance genes and the shared resistome in pig, chicken, and human feces. *Environ. Sci. Technol.* **50**, 420–427 (2016).
71. Finn, R. D. et al. Pfam: the protein families database. *Nucleic Acids Res.* **42**, D222–D230 (2014).
72. *Water Quality – Determination of Iron-phenanthroline Spectrophotometry* HJ/T 345-2007 (in Chinese) (Ministry of Ecology and Environment of the People's Republic of China, 2007).
73. *China Climate Bulletin in 2019* (in Chinese) (China Meteorological Administration, 2020).
74. Mitchell, A. L. et al. MGnify: the microbiome analysis resource in 2020. *Nucleic Acids Res.* **48**, D570–D578 (2019).
75. Buchfink, B., Xie, C. & Huson, D. H. Fast and sensitive protein alignment using DIAMOND. *Nat. Methods* **12**, 59–60 (2015).

Acknowledgements

The authors greatly thank the National Natural Science Foundation of China (grants 51878596, 41991332 and 21577123), the Natural Science Funds for Distinguished Young Scholar of Zhejiang Province (LR17B070001) and the National Key Technology R&D Program (2018YFC1802203) for their financial support.

Author contributions

L.-D.S. conceived and conducted the incubations with soil inocula, performed and analysed metagenomics and other bioinformatics, evaluated and arranged the results, and drafted the manuscript; T.G. took natural samples, measured physicochemical characteristics and quantified the functional genes/transcripts; P.-L.L. and Z.-F.N. helped perform the experiments inoculated by soil samples and microcosm incubations; Y.-J.Z.

performed the microcosm incubations; X.-J.T. supervised the project, conceived the experiments and wrote the manuscript; P.Z., L.-Z.Z., Y.-G.Z. and A.K. assisted in design and set-up of the project and contributed to the manuscript preparation; H.-P.Z. initiated and supervised the project, conceived the experiments and wrote the manuscript; all authors contributed to revising the manuscript.

Competing interests

The authors declare no competing interests.

Additional information

Extended data is available for this paper at https://doi.org/10.1038/s41561-020-00659-z.

Supplementary information is available for this paper at https://doi.org/10.1038/s41561-020-00659-z.

Correspondence and requests for materials should be addressed to X.-J.T. or H.-P.Z.

Peer review information Primary Handling Editors: Clare Davis; Xujia Jiang.

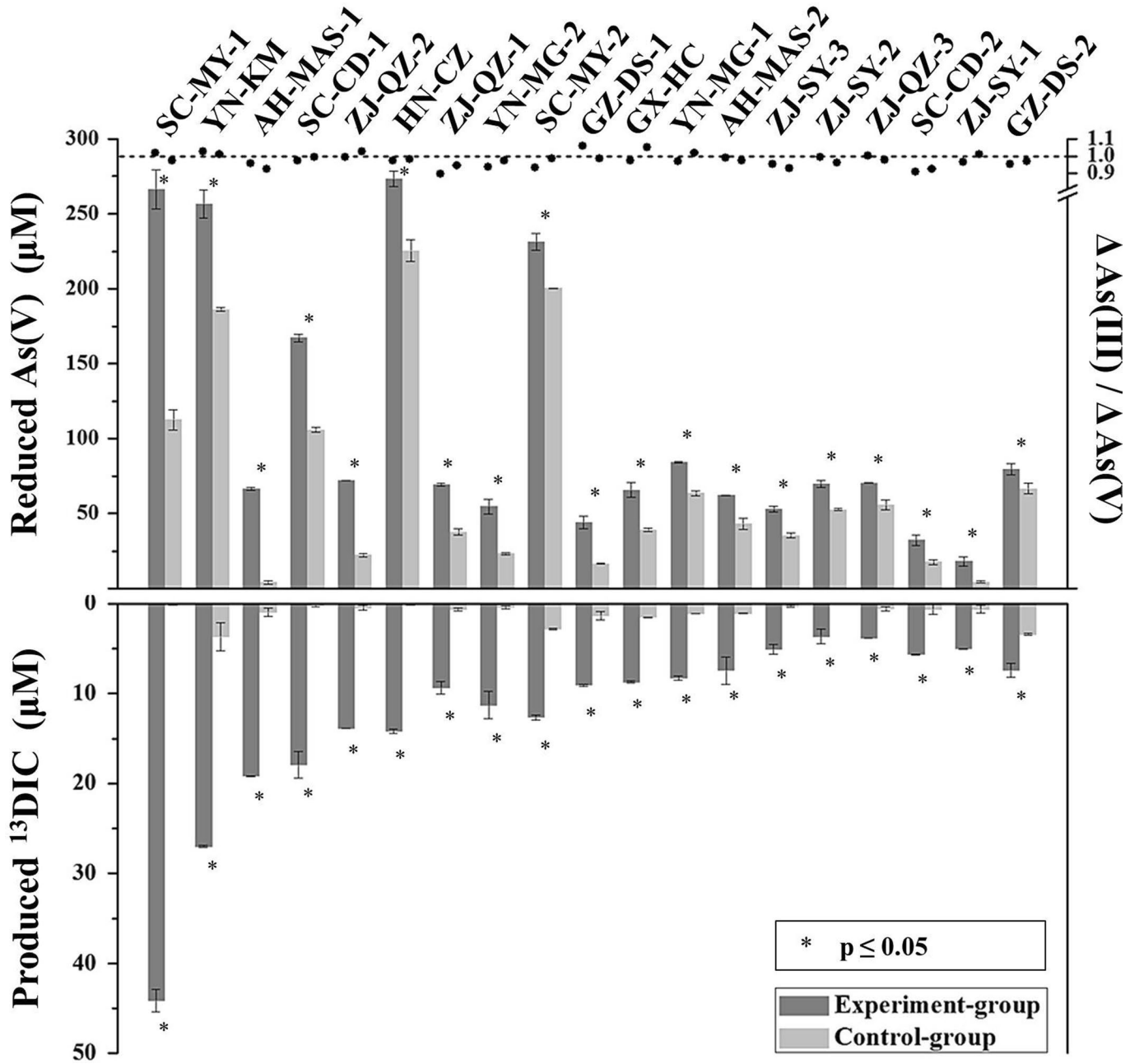

Extended Data Fig. 1 | Reduced As(V) and produced ^{13}DIC of experiments inoculated by soil samples during the whole incubation (7 days). The main differences between these two groups are $^{13}CH_4$ (top comparison) and As(V) (bottom comparison), respectively. Error bars indicate standard deviations of triplicate setups. The value of ΔAs(III)/ΔAs(V) represents the ratio of increased dissolved As(III) to decreased dissolved As(V). Asterisks indicate the statistical significance of the difference between experiment setups and corresponding control setups calculated by Kruskal-Wallis test.

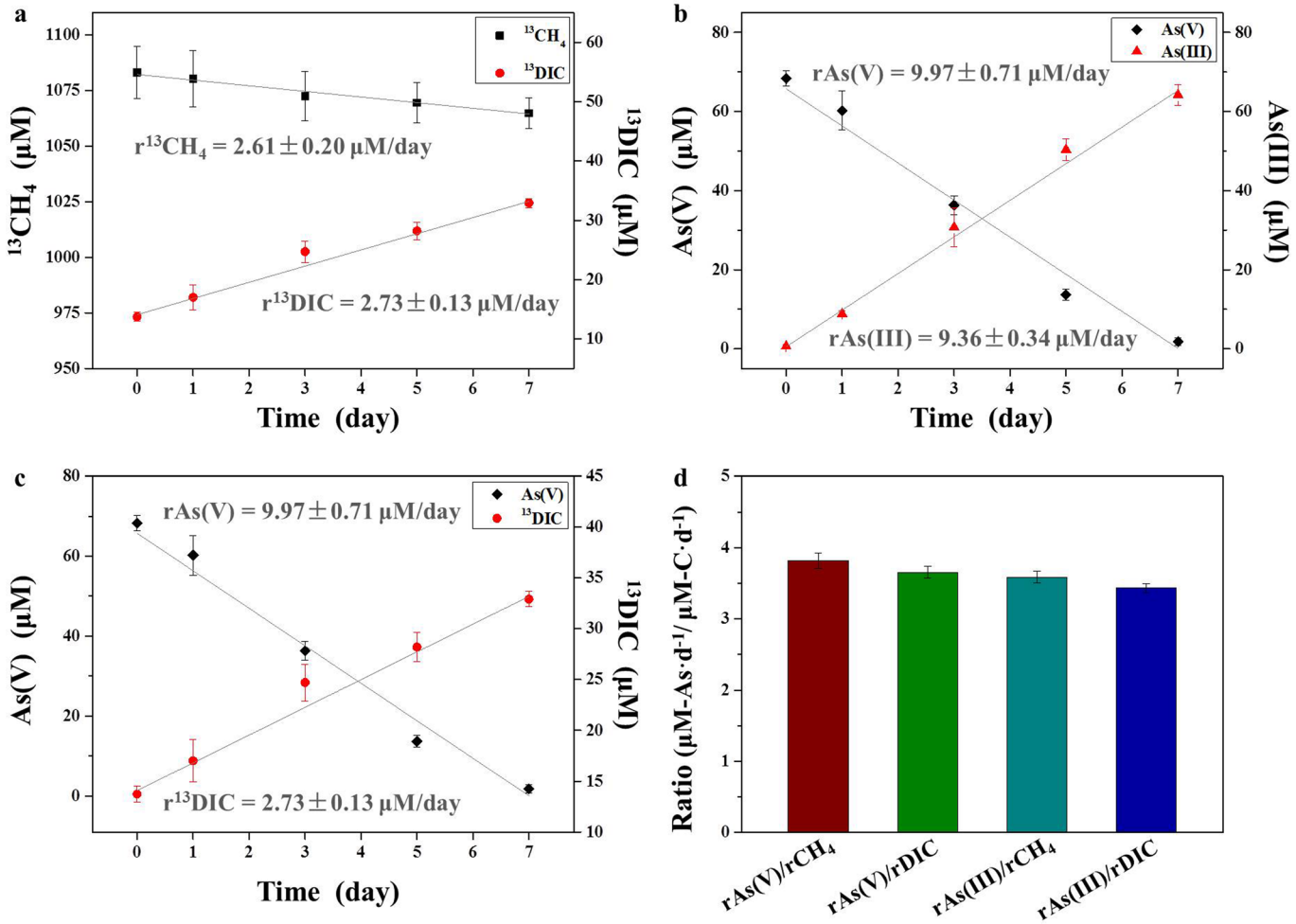

Extended Data Fig. 2 | Stoichiometry and kinetics of AOM-AsR for the AH-MAS-1 soil sample. Mass balance was tested for $^{13}CH_4$ (**a**) and As(V) (**b**). Electron balance between $^{13}CH_4$ oxidation and As(V) reduction was studied in terms of rate (**c**) and ratio (**d**). Error bars indicate standard deviations of triplicate setups. The confidence levels for fitting curves are 95%. Please note the different y-axis scales for different items.

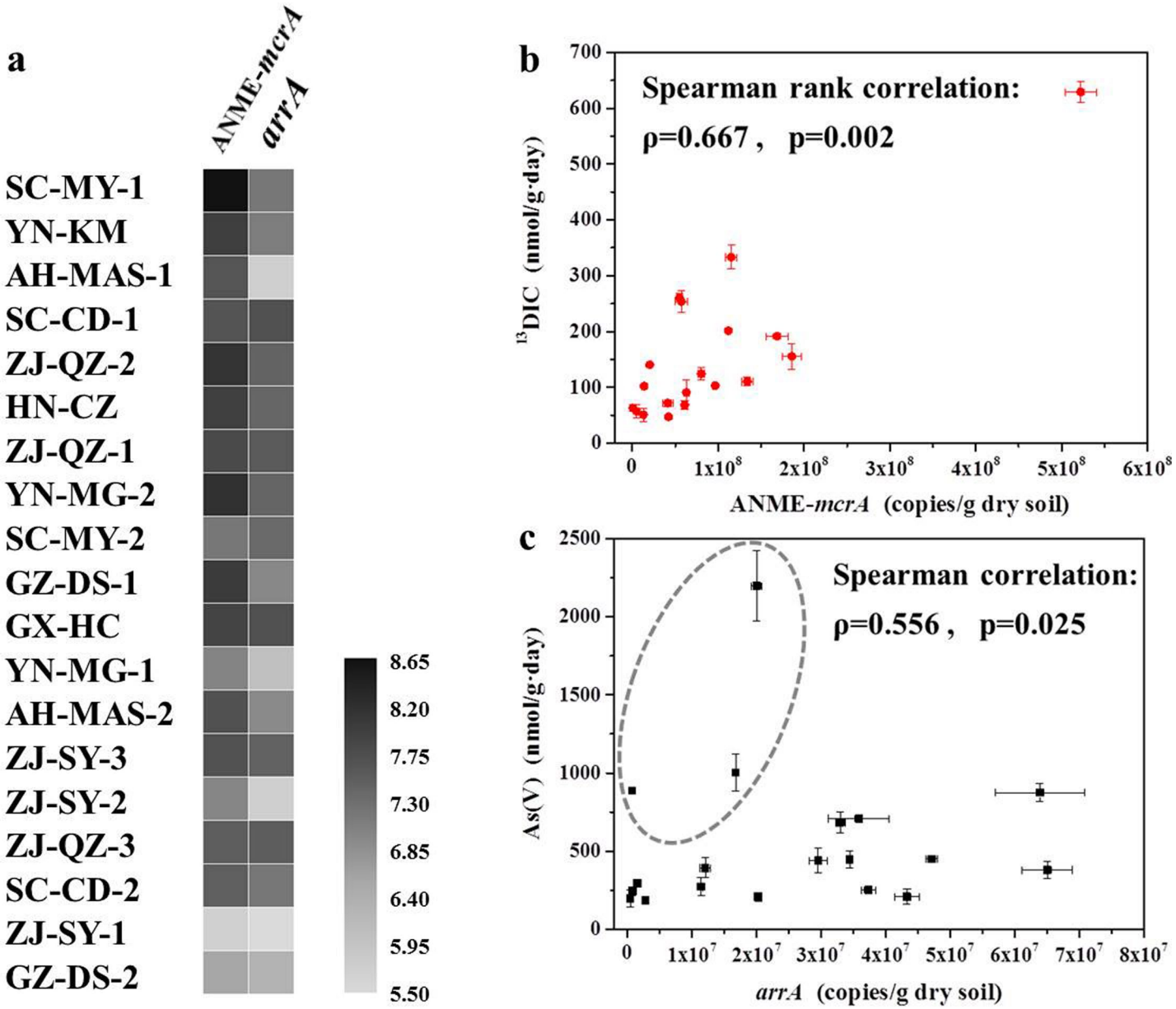

Extended Data Fig. 3 | Gene abundance and correlation with methane oxidation and arsenate reduction rates. Absolute abundances of *mcrA* and *arrA* (copies/g dry soil) were normalized by logarithm with a base of ten (**a**). Gene abundances and reaction rates were correlated using Spearman rank correlation (**b** and **c**), where ρ and p indicate the correlation efficiency and statistic probability, respectively. Error bars indicate standard deviations of triplicates. The points (SC-MY-1, YN-KM, and AH-MAS-1) in the grey circle (c) of which standard residual is 2-fold more than the standard deviation are removed based on Casewise Diagnostics. Their relatively high ATL values might explain why As(V) could be reduced rapidly at low *arrA* abundances (Supplementary Fig. 4).

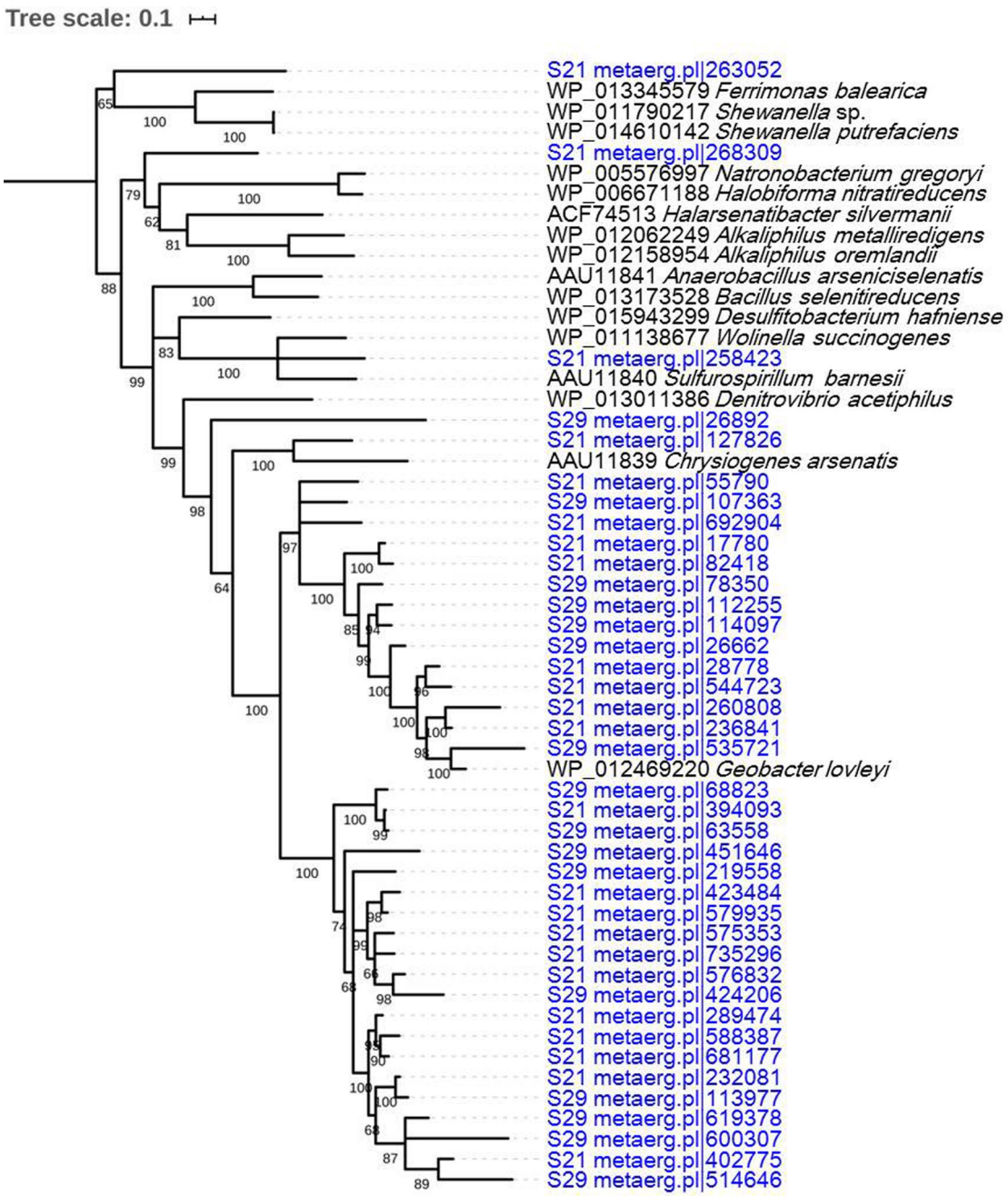

Extended Data Fig. 4 | Detailed phylogeny of respiratory arsenate reductase. The proteins recovered in this study are highlighted in purple. Bootstrap values are generated from 100 replicates. The scale bar represents amino acid changes.

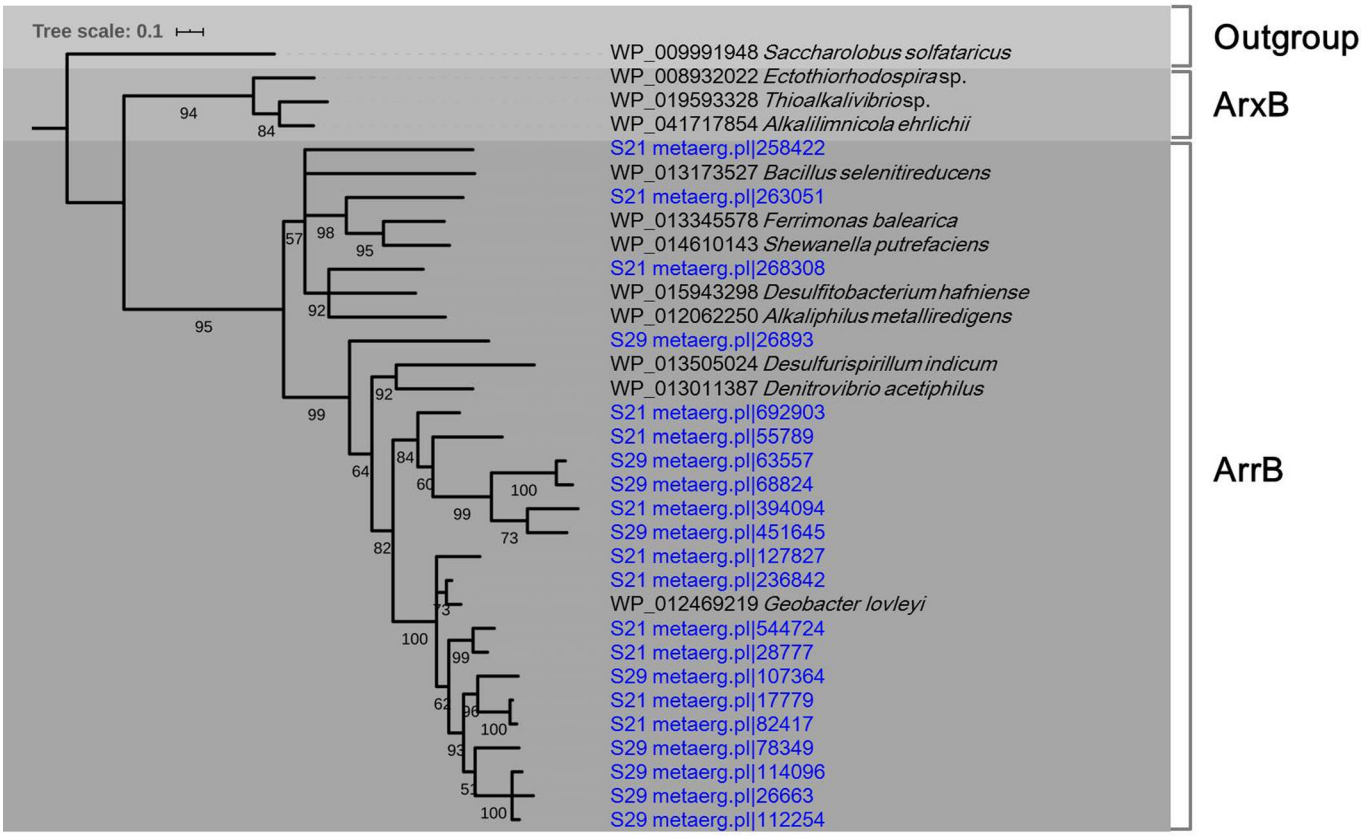

Extended Data Fig. 5 | Phylogeny of respiratory arsenate reductase beta subunit (ArrB) and closely related anaerobic arsenite oxidase beta subunit (ArxB). The proteins recovered in this study are highlighted in purple. A 4Fe-4S ferredoxin is used as the outgroup. Bootstrap values are generated from 100 replicates. The scale bar represents amino acid changes.

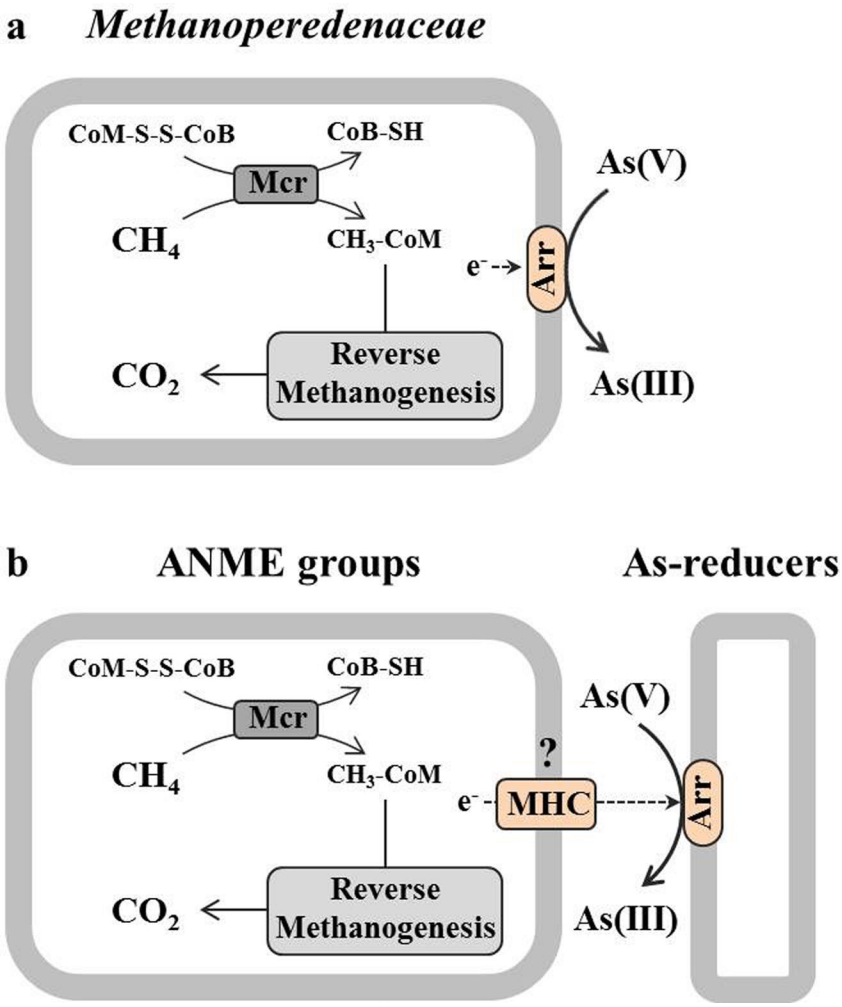

Extended Data Fig. 6 | Putative metabolic pathways of AOM-AsR. *Methanoperedenaceae* members perform AOM-AsR independently using arsenate reductase acquired through lateral gene transfer (**a**). Electrons are generated from methane oxidation via the reverse methanogenesis pathway in ANME groups, and then transferred to arsenate reducers possibly through multi-haem cytochromes (**b**). Abbreviations: Mcr, methyl-coenzyme M reductase; MHC, multi-haem cytochrome; Arr, respiratory arsenate reductase.

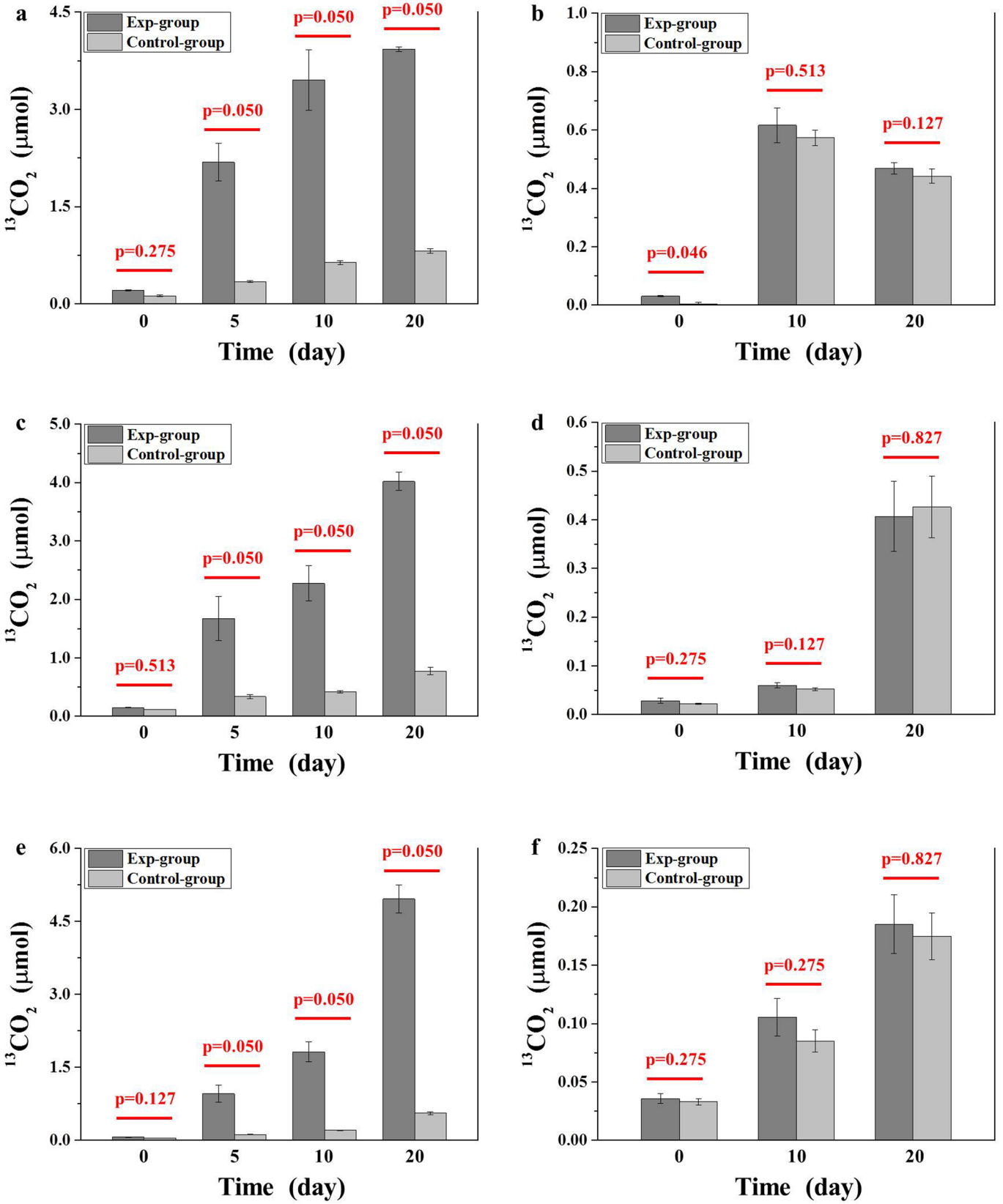

Extended Data Fig. 7 | Contents of $^{13}CO_2$ in the headspace in the microcosm incubations. (**a**), (**c**), and (**e**) are incubated with YN-MG-2, SC-CD-1, and SC-MY-2, respectively, while (**b**), (**d**), and (**f**) use the corresponding autoclaved samples. The dark and light grey in each figure indicate the experimental setups amended with environmentally relevant concentrations of $^{13}CH_4$, and the control setups without methane addition, respectively. The probability (i.e. p-values) of the differences between two setups was calculated using Kruskal-Wallis test. Error bars indicate standard deviations of triplicate setups.

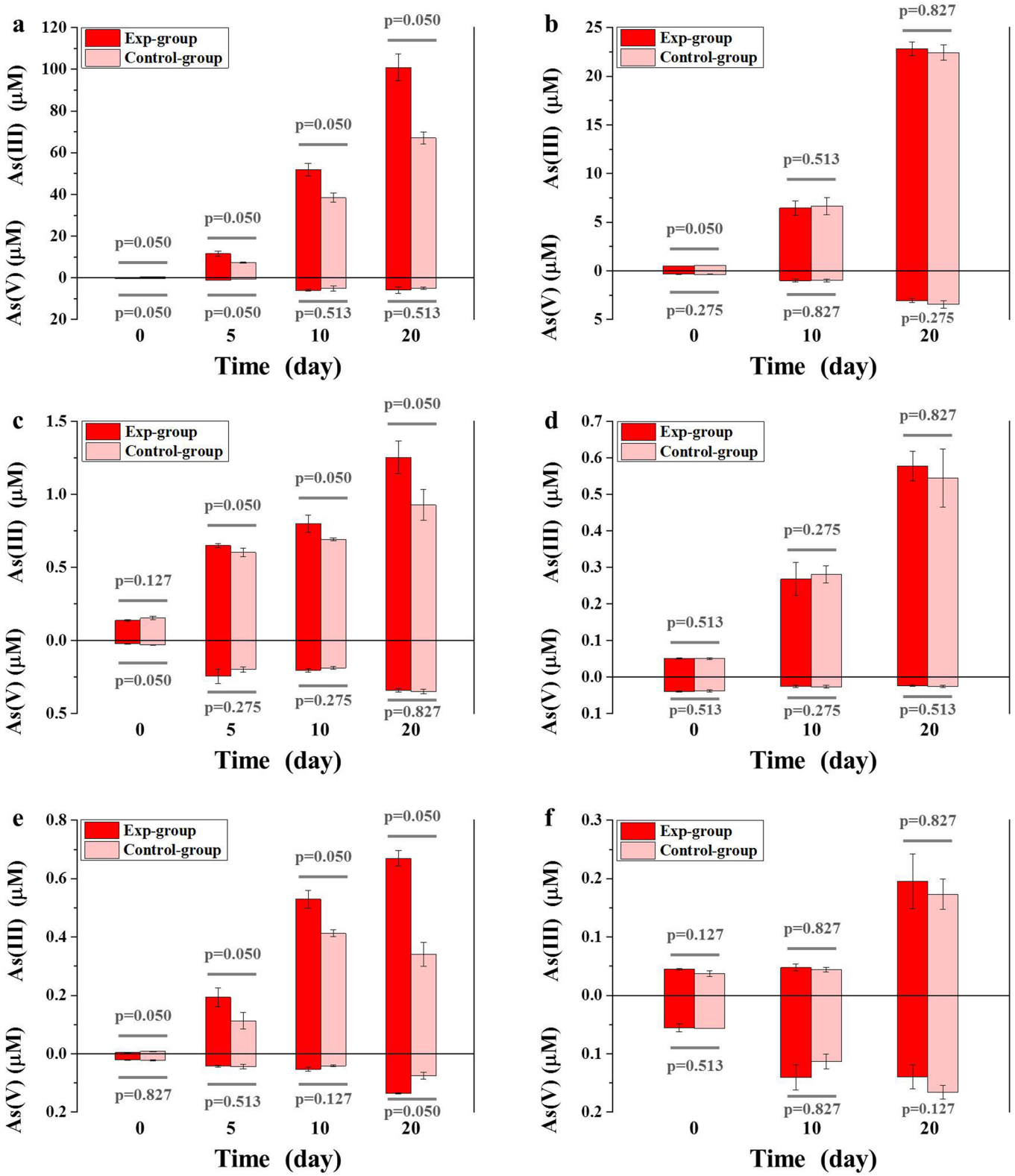

Extended Data Fig. 8 | Concentrations of As(V) and As(III) in the porewaters in the microcosm incubations. (**a**), (**c**), and (**e**) were incubated with YN-MG-2, SC-CD-1, and SC-MY-2, respectively, while (**b**), (**d**), and (**f**) show the corresponding autoclaved samples. The dark and light red in each figure indicate the experimental setups amended with environmentally relevant concentrations of $^{13}CH_4$, and the control setups without methane addition, respectively. The upper parts show As(III) while the bottom ones show As(V). Please note the different y-axis scales in the different panels. The probability (i.e. p-values) of differences between two setups was calculated using Kruskal-Wallis test. Error bars indicate standard deviations of triplicate setups.

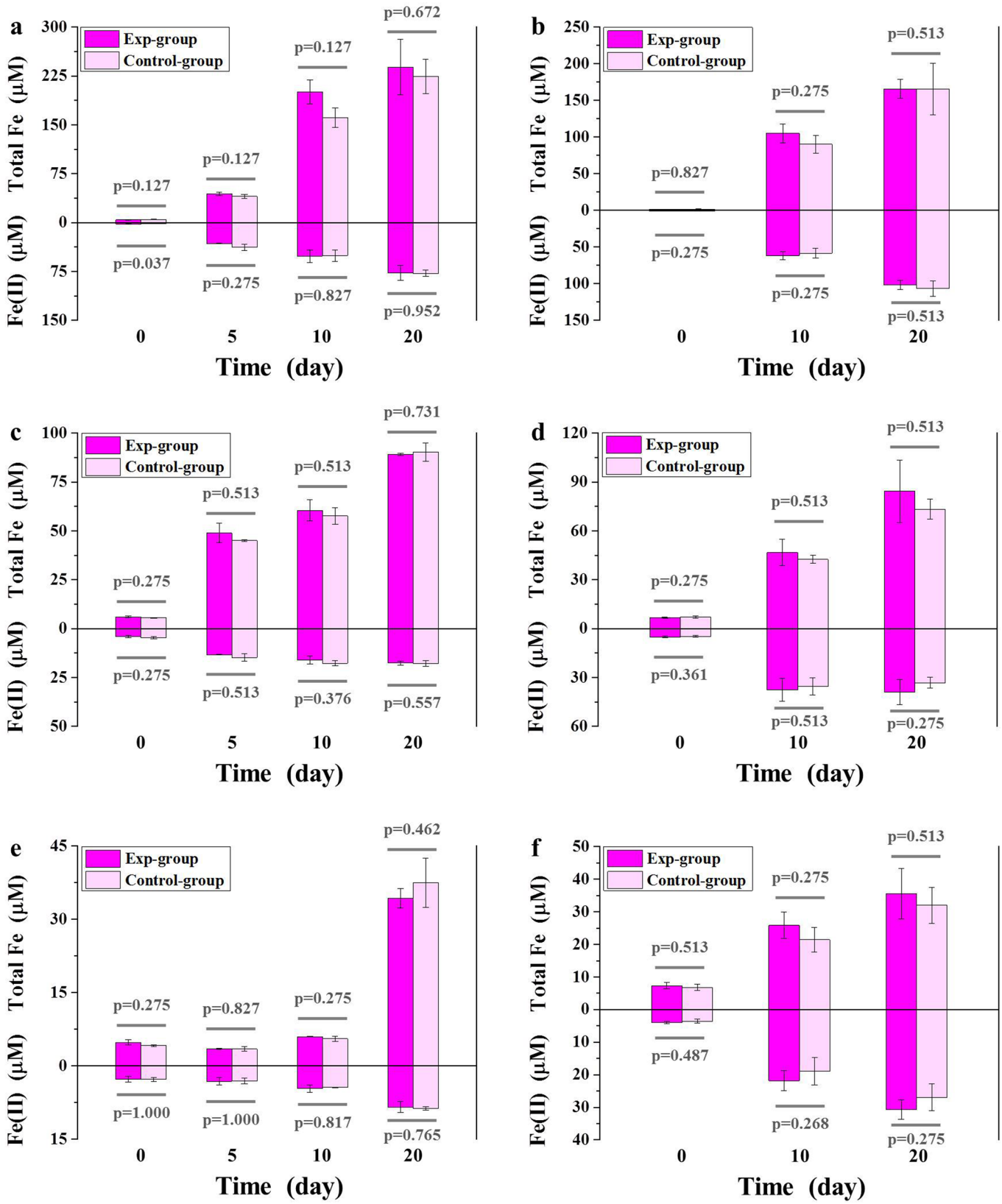

Extended Data Fig. 9 | Concentrations of total Fe and Fe(II) in the porewaters in the microcosm incubations. (**a**), (**c**), and (**e**) were incubated with YN-MG-2, SC-CD-1, and SC-MY-2, respectively, while (**b**), (**d**), and (**f**) used the corresponding autoclaved samples. The dark and light pink in each figure indicate the experimental setups amended with environmentally relevant concentrations of $^{13}CH_4$, and the control setups without methane addition, respectively. The upper parts show total Fe while the bottom ones show Fe(II). Please note the different y-axis scales in the different panels. The probability (i.e. p-values) of differences between two setups was calculated using Kruskal-Wallis test. Error bars indicate standard deviations of triplicate setups.

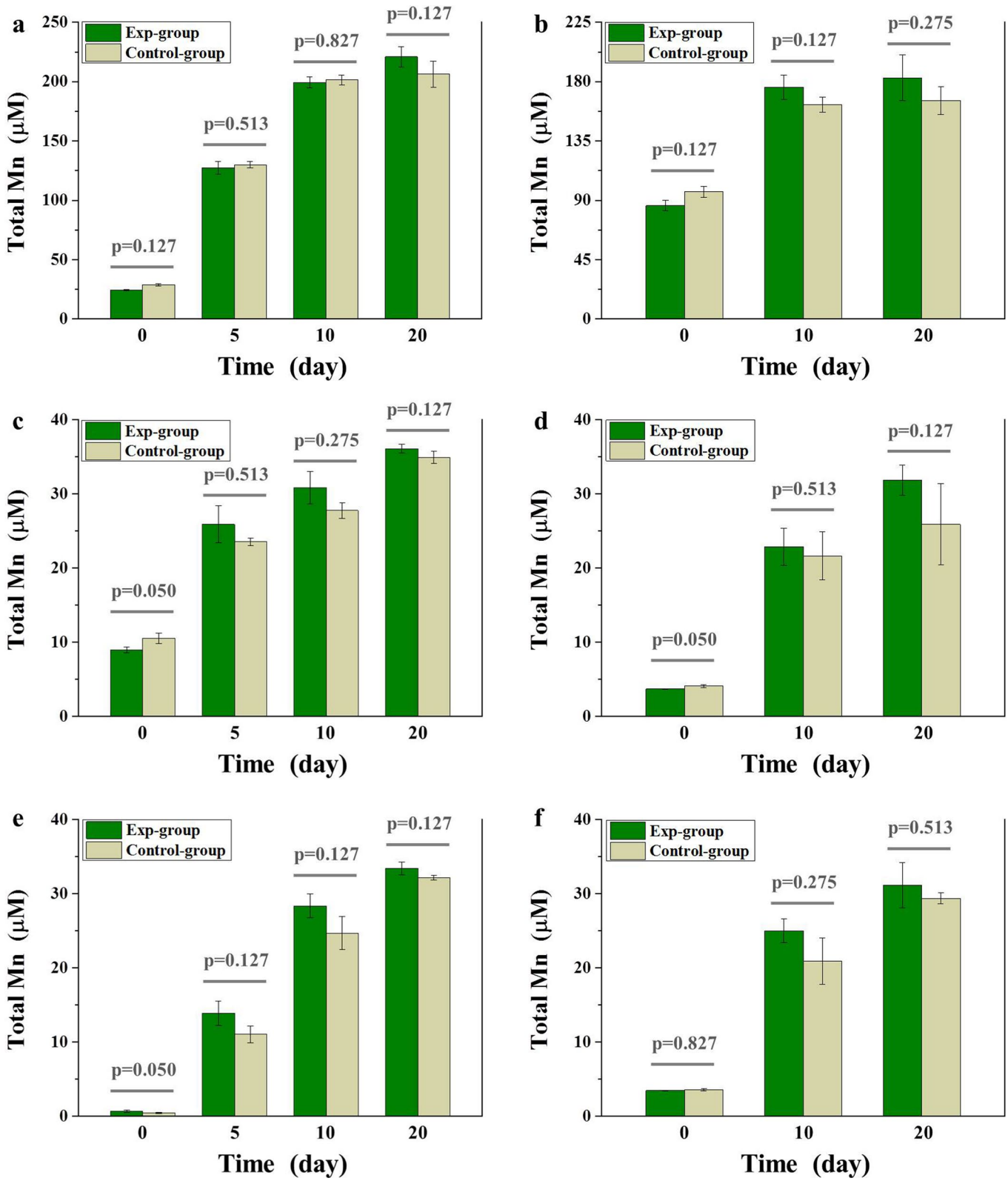

Extended Data Fig. 10 | Concentrations of total Mn in the porewaters during the microcosm incubations. (**a**), (**c**), and (**e**) were incubated with YN-MG-2, SC-CD-1, and SC-MY-2, respectively, while (**b**), (**d**), and (**f**) used the corresponding autoclaved samples. The dark and light green in each figure indicate the experimental setups amended with environmentally relevant concentrations of $^{13}CH_4$, and the control setups without methane addition, respectively. The probability (i.e. p-values) of differences between two setups was calculated using Kruskal-Wallis test. Error bars indicate standard deviations of triplicate setups.